

Radio studies of the Galactic Centre – II. The arc, threads and related features at 90 cm (330 MHz)

K. R. Anantharamaiah

Raman Research Institute, Bangalore 560 080, India

A. Pedlar

Nuffield Radio Astronomy Laboratories, Jodrell Bank, Macclesfield, Cheshire SK11 9DL

R. D. Ekers

Australia Telescope, CSIRO, Epping, NSW, Australia

W. M. Goss

National Radio Astronomy Observatory, Socorro, New Mexico 87801, USA

Accepted 1990 October 17. Received 1990 October 3; in original form 1990 August 13

SUMMARY

We present 90-cm VLA* observations of a $\sim 2^\circ \times 2^\circ$ field around the Galactic Centre. The full field was mapped with a resolution of 100×64 arcsec², and smaller regions with resolutions as high as 14×9 arcsec². The resulting images contain most of the unique features associated with the Galactic Centre, which include the Arc and its linear filaments, the arched filaments, the ‘threads’, the thermal ‘spiral’ Sgr A West, the non-thermal source Sgr A East and Sgr C. When compared to higher-frequency observations there are, however, significant differences which we mostly attribute to the increasing optical depth of the thermal components.

We show that most of the linear filaments of the Arc in the vicinity of G0.16 – 0.15, although non-thermal, have an intrinsically positive 90/20-cm spectral index ($\alpha \sim +0.3$, where flux density $S \propto \nu^\alpha$), although at least one of the filaments shows a 90/20-cm spectral index of -0.4 . The thermal feature G0.18 – 0.04 is seen in absorption, showing clearly that it is in front of the Arc. The positive latitude portion of the Arc is embedded in an extended region of ionized gas with an emission measure $> 10^5$ pc cm⁻⁶.

The ‘threads’ show up as prominently as the Arc at 90 cm. Other isolated linear features in this region, e.g. G359.54 + 0.18, G359.80 + 0.17 and Sgr C, appear similar to the threads. The 90/20-cm spectral index of three of these features is relatively steep ($\alpha \sim -0.6$) and the filament in Sgr C has $\alpha = -0.55 \pm 0.4$, whereas the ‘thread’ passing just north of Sgr A (G359.96 + 0.09) has a flat 90/20-cm spectral index. Hence there appear to be two classes of non-thermal filaments. The first class, the majority of which occur in the Arc, have flat or inverted spectra in which relativistic electrons must be produced, possibly in situ, on time-scales of less than 10^4 yr. The other class, which includes most of the isolated linear features, have relatively steep spectra and need not be directly associated with sources of relativistic particles.

Two features observed at wavelengths longer than 1 m, namely the northern galactic lobe and the low-frequency jet, do not appear as distinct features at 90 cm. We suggest that these emission areas are caused by ‘windows’ in an otherwise optically thick thermal gas.

*The Very Large Array (VLA) is part of the National Radio Astronomy Observatory, which is operated by Associated Universities Inc., under a co-operative agreement with the NSF.

1 INTRODUCTION

Radio studies of the Galactic Centre with high angular resolution have revealed a variety of unique thermal and non-thermal structures in this region (see Yusef-Zadeh & Morris 1987a,b,c). In a previous paper (Pedlar *et al.* 1989, hereafter Paper I), we have presented 90-cm VLA observations and discussed the properties of the central 10-arcmin region which contains the Sagittarius A (Sgr A) complex. This region includes the non-thermal source Sgr A East, the thermal ‘spiral’ Sgr A West and the diffuse 7-arcmin halo surrounding them. At 90 cm, the half-power primary beam of the VLA antennas is $\sim 2.6'$ and hence, in principle, it is possible to image structures within a $\sim 3^\circ \times 3^\circ$ field. Although most of the radio emission is believed to originate in the central regions of our Galaxy, the field includes a number of supernova remnants and H II regions along the line-of-sight. This paper will be mainly concerned with the central $\sim 1^\circ \times 1^\circ$ region which contains unique features believed to be associated with the Galactic Centre, such as the Arc and the arched filaments (Yusef-Zadeh, Morris & Chance 1984), Sgr C (Liszt 1985) and narrow ‘threads’ of radio emission stretching over 30 pc (Morris & Yusef-Zadeh 1985). These features have been investigated mainly at 20 cm (Yusef-Zadeh 1986; Liszt 1985) and a 30-arcmin region around the Sgr A complex has been studied at 36 cm (843 MHz) by Mills & Drinkwater (1984). Apart from the Sgr A complex (Paper I and Yusef-Zadeh *et al.* 1986a), the extended field around the Galactic Centre has not been studied with high angular resolution at low frequencies.

Imaging a single large field at 90 cm, rather than a number of individual smaller fields (e.g. ~ 30 arcmin at 20 cm), has obvious advantages when investigating the Galactic Centre region which contains many large-scale features. Furthermore, as emphasized in Paper I, in addition to providing the spectral index of the non-thermal features, the 90-cm observations are sensitive to thermal components because of their increasing optical depth at low frequencies. (At 90 cm, thermal gas at $\sim 10^4$ K has a free-free optical depth of unity if its emission measure is $\sim 3 \times 10^5$ pc cm $^{-6}$.) Hence foreground thermal gas appears as regions of absorption against the strong background non-thermal continuum. This method was used successfully in Paper I to obtain the relative locations of Sgr A East, Sgr A West and the 7-arcmin halo along the line-of-sight. The 90-cm observations are particularly valuable in view of the flat spectrum which appears characteristic of many of the non-thermal features in this region (Yusef-Zadeh *et al.* 1984; Reich *et al.* 1988). At high frequencies, these features have spectral indices similar to that of optically thin thermal free-free emission. At low frequencies, however, true thermal emission becomes increasingly optically thick and its spectral index α (where flux density $S \propto \nu^\alpha$) becomes positive ($\sim +2$ for $\tau \gg 1$). This behaviour distinguishes it from the flat spectrum non-thermal emission. At 90 cm the free-free absorption does not completely obscure the non-thermal emission from the central region, whereas at longer wavelengths (e.g. 246-cm observations by Kassim, LaRosa & Erickson 1986) the free-free optical depth is so large that it hinders studies of the structure near the Galactic Centre.

The data presented in this paper represent a significant advance in low-frequency observations of the region around the Galactic Centre. Previously, a strip brightness distribu-

tion of the Sgr A complex, at 90 cm (327 MHz), was obtained by Gopal-Krishna *et al.* (1972) with a resolution of ~ 55 arcsec using a lunar occultation technique. A 1° field around Sgr A was mapped at 73 cm (408 MHz) by Little (1974) with a resolution of 2.9 arcmin. A smaller region around Sgr A has been studied at 90 cm with higher resolution (56 arcsec) by Yusef-Zadeh *et al.* (1986a). Coarser resolution observations at wavelengths longer than 1 m have been carried out by LaRosa & Kassim (1985), Kassim *et al.* (1986) and Yusef-Zadeh *et al.* (1986a,b). The images presented in this paper cover a $\sim 2^\circ$ field with angular resolutions in the range 1.5 arcmin to 10 arcsec and have a dynamic range greater than 500:1.

In Section 2 (and Appendix A) we describe the observations and imaging methods. In Section 3, we present the properties of individual features in the extended field, and compare them with previous work. The implications of these results are discussed in Section 4.

2 OBSERVATIONS AND DATA REDUCTION

2.1 The production of images

The images presented in this paper were made from observations taken in the A, B, C and D configurations of the VLA (Thompson *et al.* 1980) and recorded in spectral line mode for the reasons outlined in Paper I. The C and D array observations are identical to those described in Paper I, although further self-calibration has considerably improved the data. New A and B configuration data were obtained in 1988 December and 1989 March, respectively. The details are presented in Appendix A. The four-configuration data were used in different combinations to obtain large-field images with different resolutions.

Radio synthesis imaging of large fields at low frequencies has a number of practical problems. These include smearing of images at large distances from the field centre due to the effects of finite bandwidth and integration times, and the distortions introduced by non-coplanar baselines (Cotton 1989; Thompson 1989). The first two problems can be corrected for, relatively simply (albeit with large computational overheads), by using single or multiple narrow bandwidths and short integration times (see Bridle 1989), while problems caused by non-coplanar baselines require careful data reduction which is described in Appendix A. Due to the prohibitive computing requirements, we have not attempted combining all the four-configuration spectral line data to make a single (8000×8000 pixels) image. Instead, we made three images with different resolutions, cell sizes and field sizes, together with a number of sub-images with various phase centres. The first image, shown in Fig. 1, included only the C and D array data, and has a resolution of 100×64 arcsec 2 (PA = 18°). The second image, shown as contours in Fig. 2 and in grey-scale in Plate 1, was derived from a combination of the B, C and D configurations and has a resolution of 33×17 arcsec 2 (PA = -2°). Finally, the image shown in Fig. 3 (contours) and Plate 2 (grey-scale) was obtained from the A and B configuration data with a resolution of 14×9 arcsec 2 (PA = 2°) over the central $0.5'$. We shall refer to the images in Figs 1, 2 and 3 as CD, BCD and AB images, respectively. Due to the lack of short UV spacings, the CD and BCD images have reduced sensitivity to extended structures on scales $> 0.5'$. Similarly, the AB image

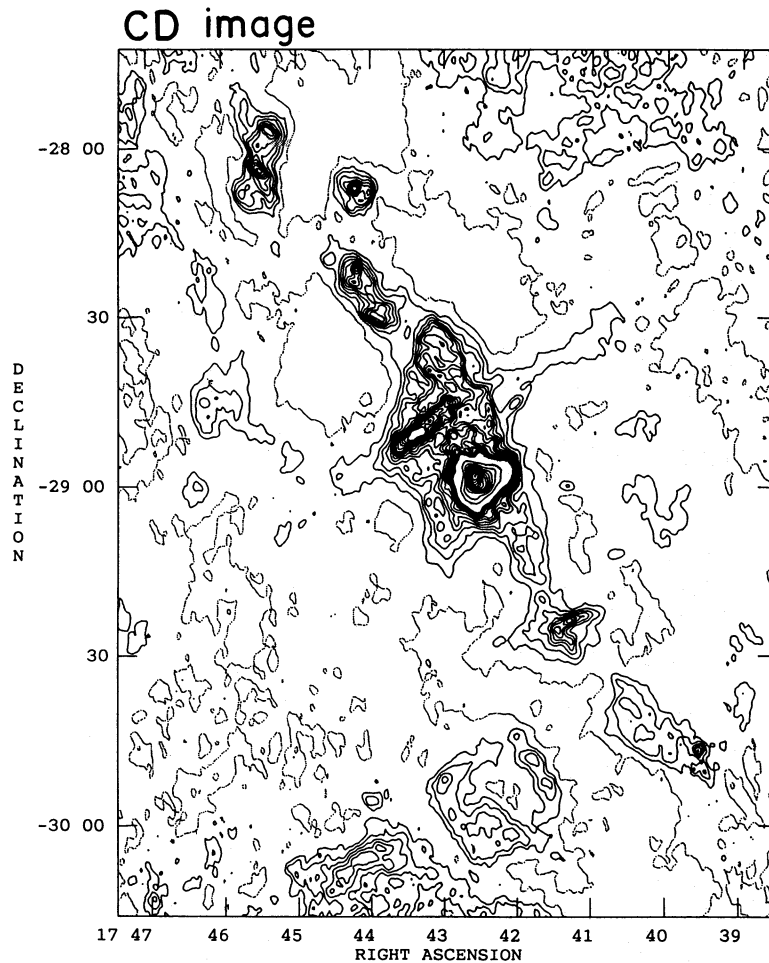


Figure 1. A contour representation of the 90-cm 'CD' image obtained using the Steer-Dewdney-Ito CLEAN deconvolution. The angular resolution is 100×64 arcsec² (PA = 18°). Contour levels are $-0.2, 0.2$ to 3.0 in steps of 0.2 , 3.0 to 45 in steps of 3 Jy beam⁻¹. The image has no sensitivity to structures > 30 arcmin.

in Fig. 3 has low sensitivity to structures larger than 5 arcmin. All the images shown in this paper have been corrected for the attenuation introduced by the primary beam response of the VLA antennas.

2.2 Comparison with previous work

The only low-frequency image of this region, comparable to Fig. 1, is the 73-cm (408 MHz) image obtained by Little (1974). All the features contained in the 73-cm image are present in our 90-cm image, but the 90-cm CD image has at least an order of magnitude greater dynamic range, higher angular resolution and covers a larger area than the 73-cm image. Hence, in order to assess the reality of faint features in the field, the only comparison which we can make is with higher-frequency surveys taken with single dishes.

The 6-cm (4.8 GHz) survey by Altenhoff *et al.* (1978) is well suited for comparison with the current image. We have therefore convolved the CD image to the 6-cm resolution (2.6 arcmin) and the resulting image is shown in galactic coordinates in Fig. 4. The main difference between the two images is the extended background evident on the 4.8-GHz image, to which the CD image is only partially sensitive. A

comparison of the two images shows that most of the 90-cm features above the 0.5 -Jy beam⁻¹ level in Fig. 4 have counterparts in the 6-cm image. These include the H II regions Sgr B1, Sgr B2, G0.8+0.2, G0.5-0.6, together with the non-thermal sources G1.05-0.1 and the shell-type supernova remnants G359.1-0.5 and G359.1-0.9. In Table 1, we give the approximate sizes and flux densities of these sources. Most of the H II regions in the field show a positive spectral index indicative of ionized gas with high free-free optical depth. The shell-type supernova remnant G359.1-0.5 has been described by Reich & Fürst (1984) and the 90-cm flux density of 32.4 Jy is consistent with the higher-frequency measurements, and implies a spectral index of -0.6 .

The central region containing the Sgr A complex and the Arc shows good structural agreement with the Bonn 6-cm image (see Fig. 4), despite more than a decade difference in observing frequency. There is, however, a marked depression in the positive latitude part of the Arc (near $l=0^{\circ}14$, $b=0^{\circ}05$) at 90 cm. As we shall discuss in Section 3.2, this depression is almost certainly caused by free-free absorption by an extended region of ionized gas. It is interesting to note that, whereas the extension of Sgr C to positive latitudes is not evident on the 6-cm image, it is clearly visible on the 90-cm image with the same resolution (see Section 3.4).

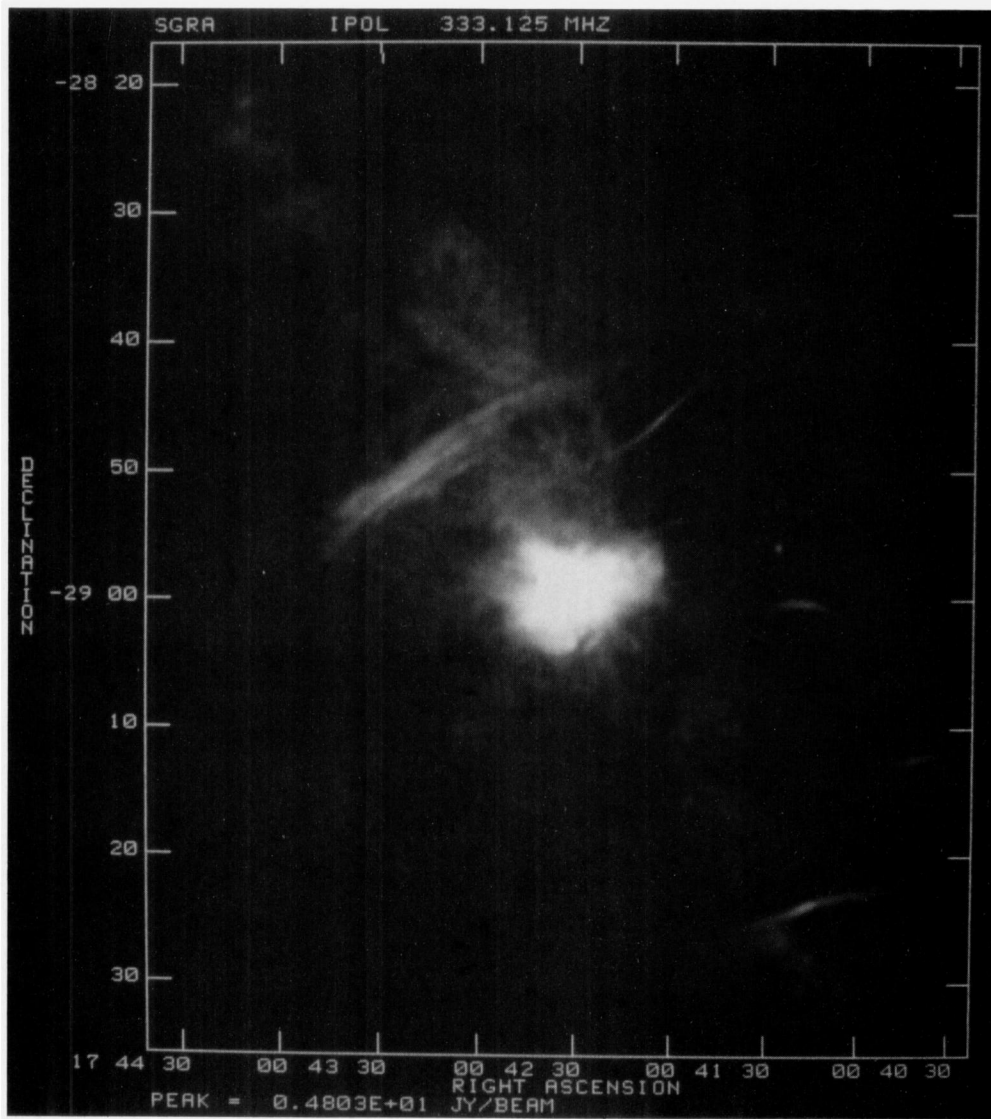


Plate 1. A grey-scale representation of the 'BCD' image.

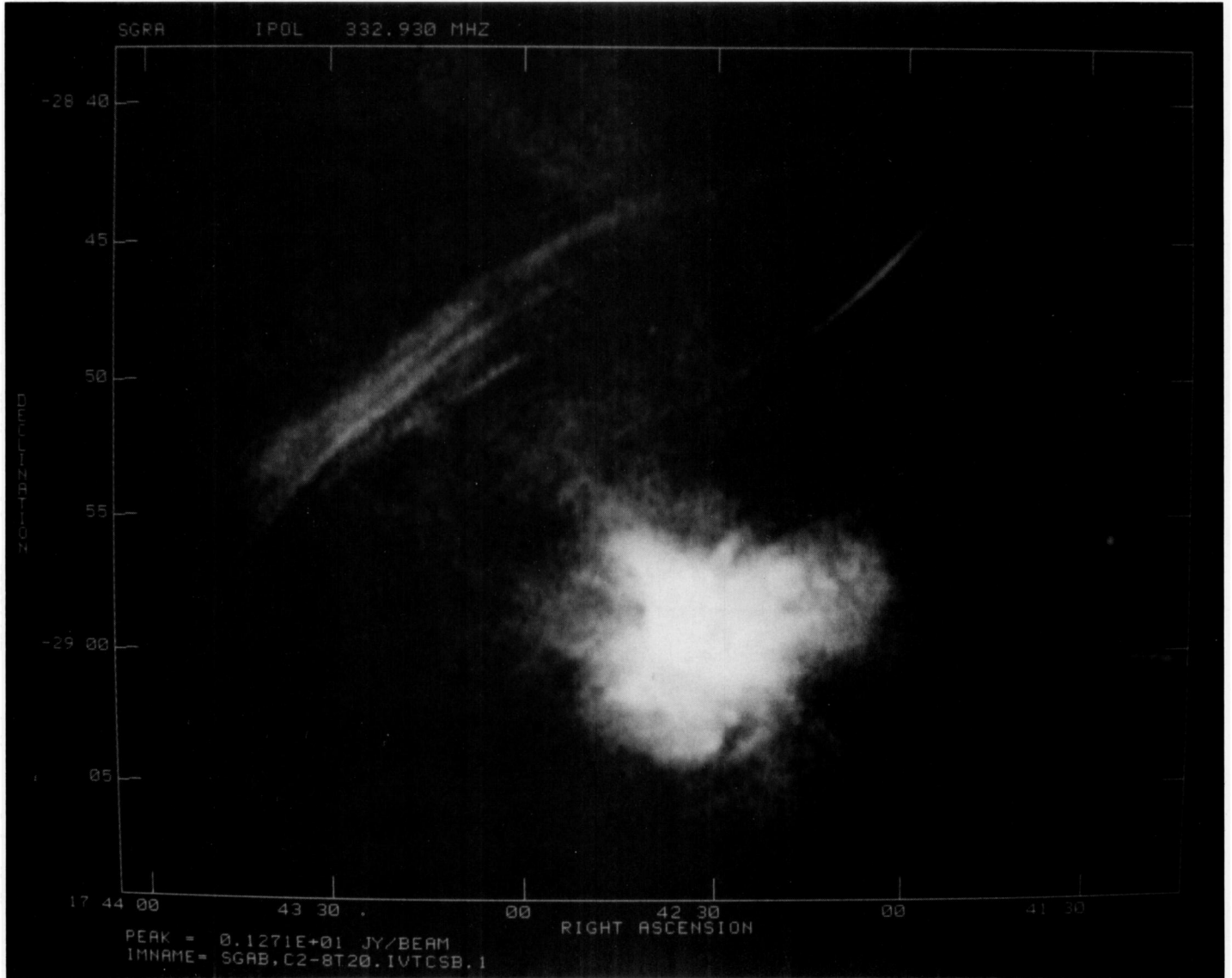


Plate 2. A grey-scale representation of the 'AB' image.

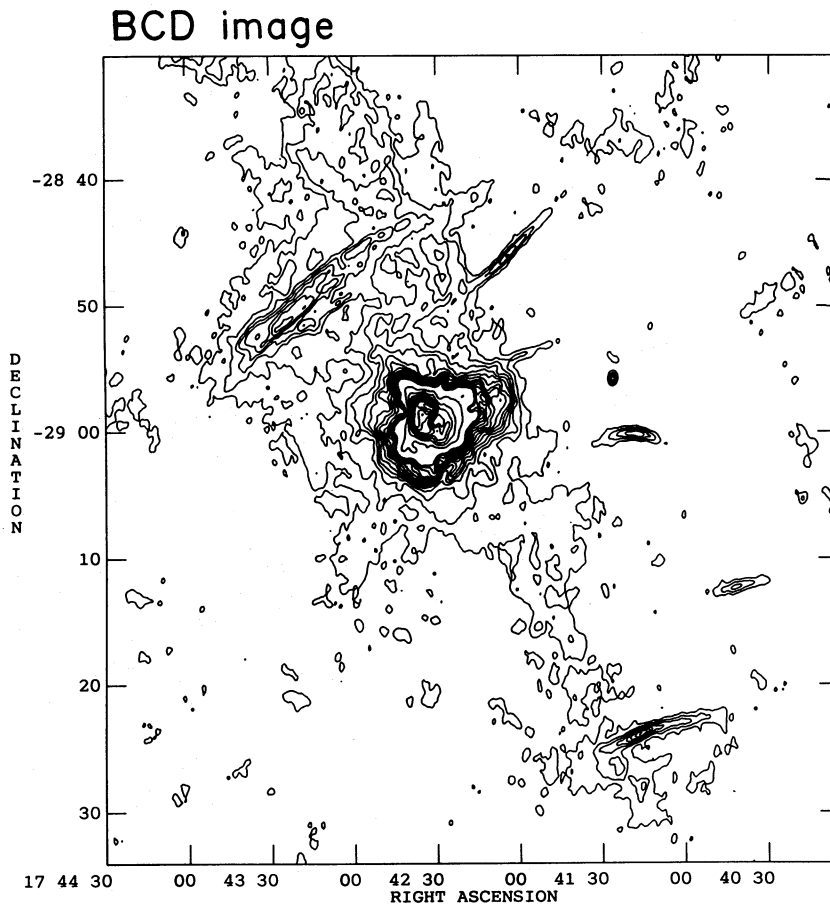


Figure 2. Contours of the 90-cm 'BCD' image obtained using the maximum-entropy deconvolution. The image has been restored with a 33×17 arcsec² beam (PA=2°). Contour levels are in units of 0.04 Jy beam⁻¹ to 0.6 Jy beam⁻¹, and 0.4 Jy beam⁻¹ thereafter.

3 RADIO FEATURES ASSOCIATED WITH THE GALACTIC CENTRE

High-resolution VLA observations of the Galactic Centre region, mainly at wavelengths shorter than 20 cm (e.g. Brown, Johnston & Lo 1981; Ekers *et al.* 1983; Yusef-Zadeh *et al.* 1984; Yusef-Zadeh 1986), have revealed many unique radio features. There is often confusion about nomenclature and in Fig. 5 we give a finding chart for identifying different components in the 90-cm images. A number of sources which do not have names are identified by their galactic coordinates in the form $Gl \pm b$. The radio features present in this region are:

- (i) the Sgr A complex, which includes the thermal 'spiral' Sgr A West, the non-thermal source Sgr A East, the 7-arcmin halo and the H II regions to the east of Sgr A East (Ekers *et al.* 1983; Yusef-Zadeh & Morris 1987a; Paper I);
- (ii) the linear Arc, located at $l=0^{\circ}18$ and lying perpendicular to the galactic plane (Yusef-Zadeh *et al.* 1984; Yusef-Zadeh & Morris 1987c) and G0.18–0.04, which crosses the Arc at right angles (Yusef-Zadeh & Morris 1987b);
- (iii) the thermal arched filaments, situated between the Arc and the Sgr A complex (Yusef-Zadeh *et al.* 1984);
- (iv) the 'threads' and other similar linear structures located mainly at positive latitudes (Morris & Yusef-Zadeh 1985; Bally & Yusef-Zadeh 1989a; Yusef-Zadeh 1989);

(v) Sgr C, located at $l=-0^{\circ}2$ consisting of a thermal source and a non-thermal filament (Liszt 1985);

(vi) the northern galactic lobe, which is an extended steep spectrum source situated 34 arcmin north of Sgr A and detected at low frequencies (LaRosa & Kassim 1985; Kassim *et al.* 1986);

(vii) and the 'low-frequency jet', which is an elongated feature to the south-east of Sgr A, detected at wavelengths longer than 190 cm (Yusef-Zadeh *et al.* 1986a; Kassim *et al.* 1986).

All the above features can be identified in our wide-field 90-cm images (Figs 1 and 2), although the northern galactic lobe and the low-frequency jet do not appear as distinct structures. We shall now discuss the above features separately.

3.1 The Sgr A complex

This region was discussed extensively in Paper I, and the present observations confirm the main conclusions of that paper. In Figs 2 and 3, the appearance of the thermal source Sgr A West in absorption clearly establishes that it is in front of the non-thermal source Sgr A East. The absence of the central source Sgr A* indicates that it is either behind or embedded in Sgr A West. A further point which can be

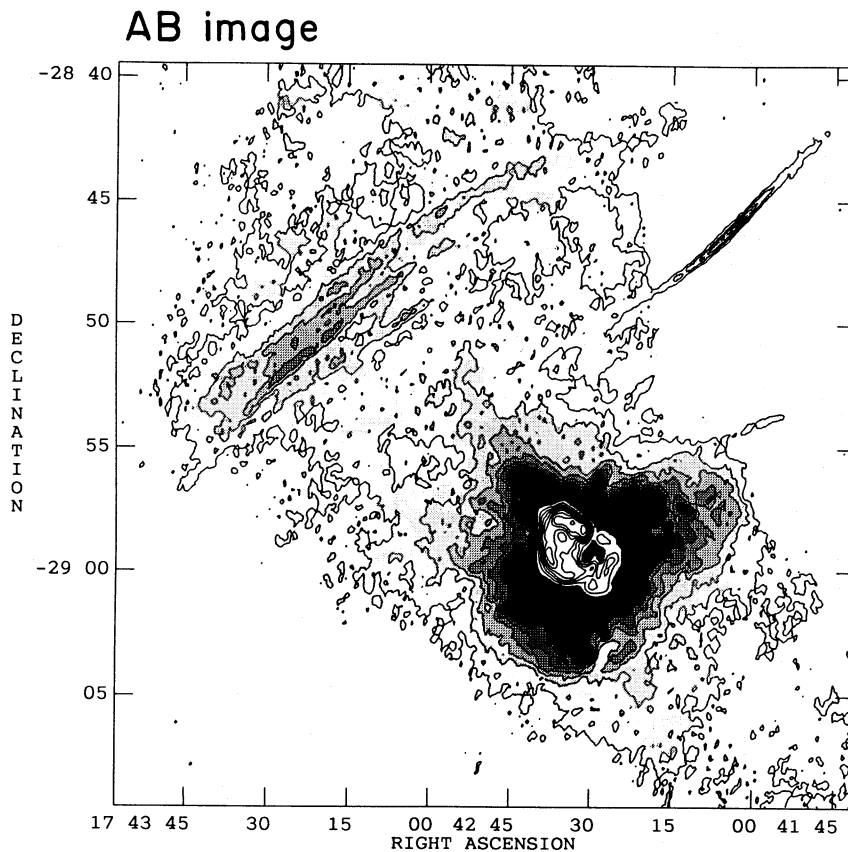


Figure 3. A contour map of the 90-cm 'AB' image obtained using the maximum-entropy deconvolution. The image has been restored with a 14×9 arcsec² beam (PA = 2°). Contour levels are in units of $0.02 \text{ Jy beam}^{-1}$ up to 0.4 Jy beam^{-1} , and 0.1 Jy beam^{-1} thereafter.

added here is that the chain of three H II regions immediately to the east of Sgr A East (Ekers *et al.* 1983) seem to be in absorption against the 7-arcmin halo (Figs 2 and 3). Although the angular resolution is not sufficient to measure the optical depth accurately, the absorption indicates that the H II regions are either in front of the halo or embedded in it. Almost all the other discrete sources in the vicinity of the Sgr A complex, which are detected at higher frequencies (e.g. sources E to J in Yusef-Zadeh & Morris 1987c), are absent in the 90-cm image. This is consistent if these sources are thermal and become optically thick at this wavelength.

3.2 The arched filaments and associated thermal components

The arched filaments are located at $l = 0^\circ 1$ and $b = 0^\circ 08$ and extend along a curve from the Arc towards the Sgr A complex (see Fig. 5). They appear prominently in the 6- and 20-cm images obtained by Yusef-Zadeh *et al.* (1984) and contain at least two distinct features, which have been designated as the 'eastern' and 'western' arched filaments by Morris & Yusef-Zadeh (1989). A recombination line study (Yusef-Zadeh, Morris & van Gorkom 1987) has shown the arched filaments to be predominantly thermal. Other thermal components in this region are G0.18–0.04, which crosses the Arc at right angles, and G0.15–0.05, which is located near the southern edge of the Arc (see Fig. 5). By virtue of their structures these two components have been referred to

as the 'sickle' and the 'pistol' by Yusef-Zadeh & Morris (1987b).

The 90-cm images (Figs 2 and 3) of the region containing the arched filaments and the associated thermal components appear very different from images at higher frequencies. A visual comparison can be seen in Fig. 6(a) and (b) where we show a portion of the BCD image (resolution 33×17 arcsec²) along with a 20-cm image obtained from Yusef-Zadeh (1986) and convolved to the same resolution. Outside the Sgr A complex the brightest parts of the 20-cm image are the eastern and western arched filaments and G0.18–0.04. At 90 cm, however, the most prominent region is in the eastern section of the Arc in the vicinity of G0.16–0.15, and the arched filaments are only marginally detected against the extended background. The difference is clearly due to the thermal nature of these regions which must have become optically thick at 90 cm. The thermal nature of these regions is also evident in Fig. 6(c) where we show the 90/20-cm spectral index obtained from Fig. 6(a) and (b). Although the spectral index image (Fig. 6c) is constructed from data which do not have similar sensitivity to structures with different scales, it can be used to identify regions of optically thick thermal emission and also compact regions with steep non-thermal spectra. The arched filaments, G0.18–0.04 and G0.15–0.05, are clearly delineated by areas of spectral index greater than unity. This is consistent with optically thick thermal emission and implies emission measures in excess of 10^5 pc cm^{-6} . Yusef-Zadeh & Morris (1987b) give

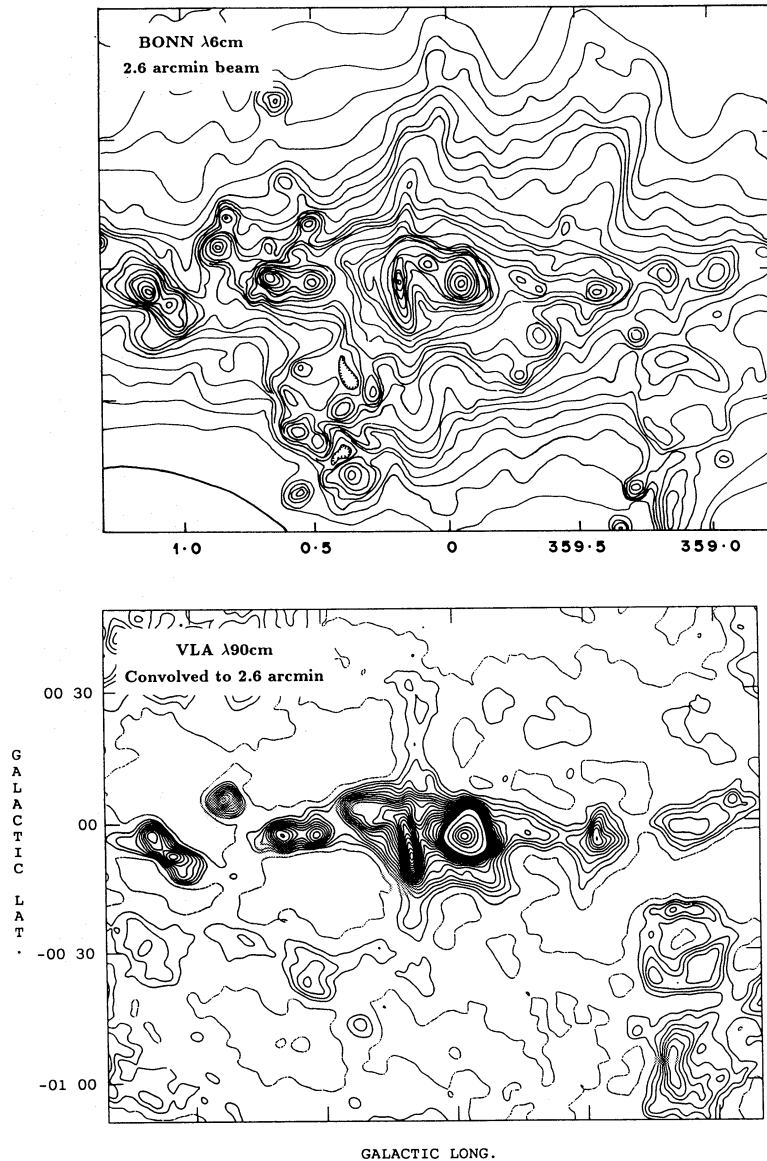


Figure 4. A comparison between the 90-cm ‘CD’ image and the 6-cm image of Altenhoff *et al.* (1978). The 90-cm image has been rotated to galactic coordinates and convolved to the 2.6-arcmin resolution of the 6-cm image. The contour levels of the 90-cm image are 0.5 Jy beam^{-1} to 12 Jy beam^{-1} and at 20, 40, 60, 80 and 100 Jy beam^{-1} thereafter.

Table 1. Parameters of the main sources in Fig. 1.

Source	RA (1950)			DEC (1950)			Flux Density Jy	Angular Size arcmin ²
	h	m	s	°	'	"		
G359.1-0.5	17 42	16.44		-29 53	45		32 ± 4	17×20
G359.0-0.0	17 40	15.2		-29 43	20		33 ± 2	7×14
G0.6-0.6	17 45	59.6		-28 44	59		20 ± 2	6×8
G1.1-0.1	17 45	29.0		-28 04	02		41 ± 2	7×16
G0.9+0.1	17 44	11.7		-28 07	17		17 ± 2	7×7
G0.34+0.05	17 43	04.7		-28 36	08		64 ± 3	12×10
Sgr C	17 41	17.3		-29 23	53		36 ± 2	9×11
Sgr B1+B2	17 44	01.4		-28 26	13		37 ± 2	7×16
Sgr A + Arc	17 42	52.8		-28 56	40		647 ± 5	21×25

the emission measure of G0.18–0.04 as $9.1 \times 10^6 \text{ pc cm}^{-6}$, and the eastern and western arched filaments have emission measures in excess of 10^5 pc cm^{-6} (e.g. Pauls *et al.* 1976).

As pointed out by Yusef-Zadeh & Morris (1987b, 1988), many thermal features such as the arched filaments, G0.18–0.04 and G0.15–0.05, appear to be physically interacting with the non-thermal linear filaments of the Arc. Since the thermal regions have become optically thick at 90 cm, it is possible to use the 90-cm images to obtain the relative location, along the line-of-sight, of the thermal components and the non-thermal Arc. In Fig. 7(a) we show cross-cuts at 20 and 90 cm along the northern edge of the Arc at the position of G0.18–0.04. This source shows strong absorption at 90 cm and the minimum brightness temperature of the absorption feature ($\sim 0.15 \text{ Jy beam}^{-1}$) is \sim

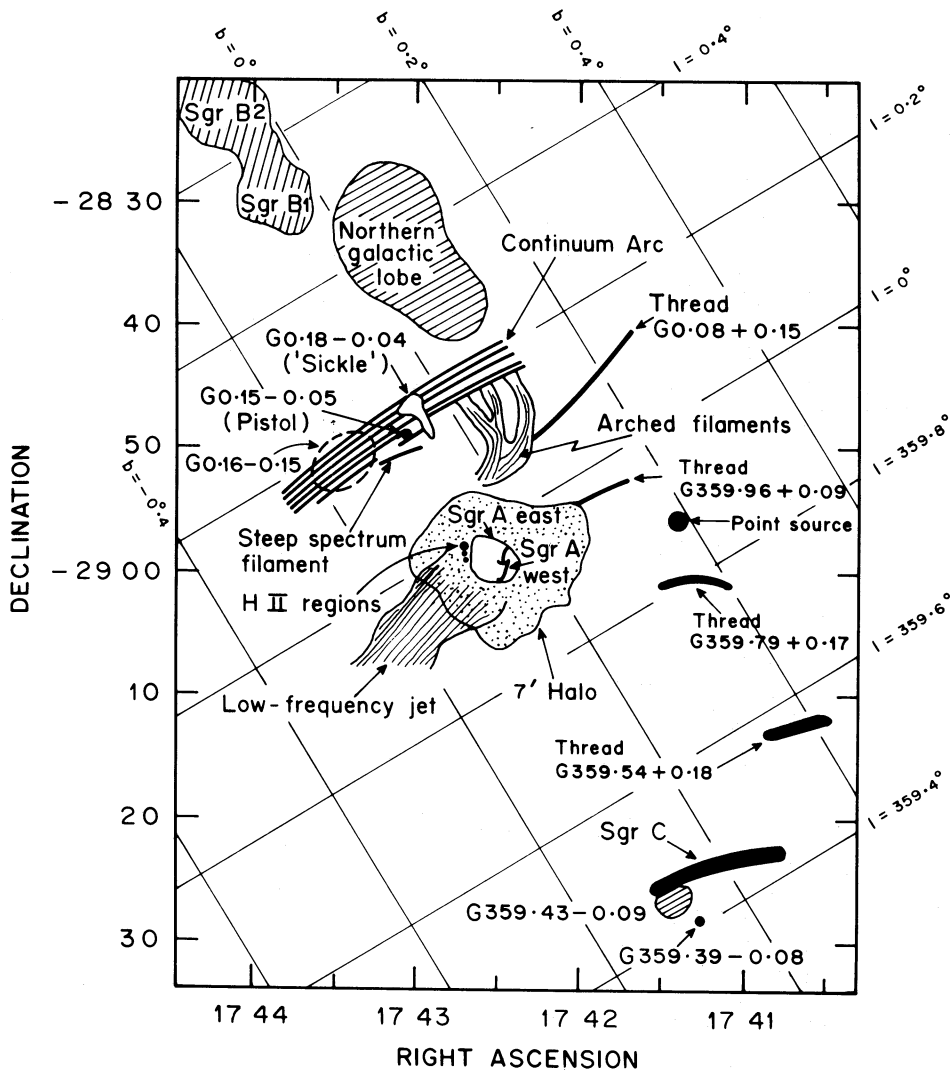


Figure 5. A schematic drawing of the radio features in the Galactic Centre region. This may be used as a finding chart for the different components in Figs 1, 2 and 3.

3000 K. This suggests that the thermal emission associated with G0.18–0.04 must be mainly in front of the non-thermal emission associated with the Arc. In Fig. 7(b), we show cross-cuts at 20 and 90 cm (from Fig. 6a and b) along the southern edge of the Arc, passing through both G0.15–0.05 and G0.18–0.04. While both these components appear prominently at 20 cm, they are completely extinguished at 90 cm due to their high optical depth. A possible shallow absorption can be seen at 90 cm at the position of G0.15–0.05, suggesting that it may also be in front of the Arc. In Fig. 7(b), only marginal absorption is observed at the extrapolated position of the eastern branch of the eastern arched filaments and no convincing absorption against the Arc at the position of the other arched filaments. As seen in Fig. 6(a) (also Figs 2 and 3), the 90-cm intensity of the linear features in the Arc decreases rapidly to positive latitudes where the arched filaments intersect the Arc. Therefore the lack of obvious absorption near this intersection cannot be used unambiguously to determine the relative geometry of these two features.

The decrease in the intensity of the Arc in the region of the arched filaments is strongly dependent on wavelength and in Fig. 7(c) we show a selection of cuts along the Arc at different wavelengths which illustrate this effect. This decrease in intensity towards positive latitudes can be explained (see also Yusef-Zadeh *et al.* 1986b) by free-free absorption by an extended component of ionized gas in this region. The 90-cm intensity of the Arc is consistent with an optical depth $\tau \sim 1$. If due to free-free absorption, this would result in $\tau \sim 8$ at 246 cm (123 MHz) which readily accounts for the low intensity of the Arc near $b \sim 0^\circ$ at this wavelength (Kassim *et al.* 1986). These optical depths imply emission measure of $\sim 10^5$ if $T_e \sim 10^4$ K. The region must be at least 10 arcmin in extent, which assuming spherical symmetry, would give an rms electron density of $\sim 50 \text{ cm}^{-3}$. Radio recombination line measurements of this region have indicated that such a component of ionized gas, showing high-velocity gradients symptomatic of an association with the Galactic Centre, extends to more positive longitudes than the Arc (e.g. Kesteven & Pedlar 1977; Pauls & Mezger 1980;

Anantharamaiah & Yusef-Zadeh 1989). The present observations suggest that most of the western part of the Arc at positive latitudes is behind or embedded in this region. However, at least two filaments can be followed at $\lambda 90$ cm to positive latitudes, which could imply that either the free-free absorption is patchy, or that these two filaments are on the nearside of the thermal component.

To summarize, the main reason for the difference in the structure of the arched filaments at 90 cm as compared to 20 cm is the high free-free optical depth of this region. The appearance of the sickle-shaped (G0.18–0.04) feature in absorption at 90 cm clearly indicates that it is on the near side of the Arc. In addition to the thermal arched filaments, there appears to be an extended component of ionized gas which reduces the intensity of the positive latitude portion of the Arc at lower frequencies.

3.3 The Arc and its linear filaments

The Arc is located at $l=0^{\circ}18$ and runs perpendicular to the galactic plane. An extensive series of images of this region at 20 and 6 cm have been described by Yusef-Zadeh (1986) and Yusef-Zadeh & Morris (1987c), which demonstrate the Arc to be composed of a series of linear filaments, together with a series of ‘helical’ filaments which appear to surround the linear filaments. The linear structures are also present at 90 cm and are particularly well defined in Fig. 3. The north and south extensions to the Arc are present in the low-resolution CD image (Fig. 1), although their prominence in this image is emphasized by the insensitivity to extended structures. At the highest resolution (Fig. 3) at least four distinct linear features in the vicinity of G0.16–0.15 are observed. In Fig. 8(a) we show cross-cuts, taken at constant galactic latitude, derived from Fig. 3 and the 20-cm image from Yusef-Zadeh (1986) after convolving both to a common resolution of 15 arcsec. These cross-cuts clearly delineate the multiple filaments and indicate that most of the filaments have a flat or positive spectral index. Higher-resolution observations by Yusef-Zadeh & Morris (1987c) show the Arc region to contain at least 15 separate filaments, and each 90-cm filament consists of several distinct components. For example the most prominent 90-cm filament (see Fig. 8a) encloses filament IV and V as defined by Yusef-Zadeh & Morris (1987b). The problems of determining an accurate baselevel for the linear filaments can be seen in Fig. 8(a) which is affected by a large contribution from ionized gas in the helical filaments at 20 cm. Nevertheless, there is no doubt that the spectral index of most of these filaments is certainly not negative and many show a positive value, in agreement with estimates made at higher frequencies (Reich *et al.* 1988). Using similar cross-cuts we have estimated the intensities of the most prominent filaments at different latitudes, and derived spectral indices which are plotted in Fig. 8(b). Although the errors are large, there is good evidence for $\alpha \sim +0.3$ in the vicinity of G0.16–0.15. The spectral index becomes even more positive ($\alpha > +0.5$) towards positive latitudes.

Most of the other filaments appear to show similar behaviour, although at least one filament, passing ~ 1 -arcmin south of G0.15–0.05 (the ‘pistol’), is anomalous and has a negative spectral index of -0.4 (see Fig. 8b). The region of negative spectral index is relatively small ($\sim 0^{\circ}05$), since an apparent

continuation of the filament to latitudes below $-0^{\circ}1$ has a positive spectral index ($\alpha \sim +0.2$). Therefore, a part of this filament may be physically separate. It may be significant that the steep-spectrum filament is out of alignment ($\sim 10^{\circ}$) with the majority of the Arc filaments.

The slightly positive spectral indices observed in most of the linear filaments of the Arc would, in many situations, be considered to be indicative of thermal emission which is becoming optically thick, but polarization measurements (e.g. Inoue *et al.* 1984; Seiradakis *et al.* 1985; Inoue *et al.* 1989; Reich 1990) have demonstrated that the linear filaments have a non-thermal origin. The 90-cm measurements also confirm the non-thermal nature of the filaments since, in some parts of the filaments, 90-cm brightness temperatures of at least 5000 K are observed (see Figs 3 and 7). If this were free-free emission from thermal gas at 10^4 K, then it would be highly optically thick and have a spectral index greater than $+1$.

As discussed in the previous section, the region of the Arc to positive latitudes is attenuated by free-free absorption, which almost certainly accounts for the increase in the 90/20-cm spectral index towards positive latitudes (Fig. 8b). There is some evidence that in this region the attenuation increases towards smaller longitudes (namely towards the arched filaments), as filament VIII of Yusef-Zadeh & Morris (1987b) (see Fig. 8a) appears to show less attenuation than other filaments in this region. This behaviour could imply that filament VIII is on the nearside of the absorbing cloud.

Although positive spectral indices in the positive-latitude half of the Arc may be due, in part, to the absorbing thermal cloud discussed above, it appears unlikely that the positive 90/20-cm spectral index ($\alpha \sim +0.3$) measured in the vicinity of G0.16–0.15 can be due to a similar effect. As can be seen in Fig. 7(c) there appears little attenuation of the 246-cm emission in this region. Yusef-Zadeh *et al.* (1986b) also find evidence for a flat spectrum for G0.16–0.15 at 190 cm. Thus, as the optical depth in this direction at 246 cm appears to be < 1 , then, given the rapid increase in free-free optical depth with wavelength ($\tau_{ff} \propto \lambda^{2.1}$), the 90-cm free-free optical depth for this region cannot be larger than ~ 0.1 . Hence the 90/20-cm spectral index for this region probably represents the intrinsic spectrum of the non-thermal emission from the Arc. A similar positive spectral index has been found by Reich *et al.* (1988) at higher frequencies. The implications of this result will be discussed in Section 4.2.

To summarize, the linear filaments of the Arc discovered by Yusef-Zadeh *et al.* (1984) are also detected at 90 cm. Most of the filaments show an intrinsically positive 90/20-cm spectral index ($\alpha \sim +0.3$), although at least part of the southernmost filament shows a negative 90/20-cm spectral index ($\alpha \sim -0.4$). The low intensity of the positive-latitude parts of the Arc, at low frequencies, is consistent with absorption by an extended cloud of ionized gas in this region.

3.4 Sagittarius C

This source was imaged separately using the A and B array data and convolved to a resolution of 23×13 arcsec². The resulting image is shown in Fig. 9. This image has the same resolution as the 18-cm image of this region by Liszt (1985), selected contours of which are also shown in Fig. 9. Apart from the differences due to the 90-cm image being less sensi-

tive to extended structure than the 18-cm image, the two images show similar features. The most striking feature is a linear structure ~ 10 arcmin in extent. By means of cross-cuts we have estimated the spectral index at a number of positions along the filament. The cross-cuts indicate a spectral index of $\sim +0.2$ near the eastern end and ~ -0.9 near the western end of the filament, and the mean value is found to be -0.55 . The flat or positive spectral index in the eastern portion may be caused by the presence of thermal gas which becomes partially optically thick at 90 cm. As the spectral index in the western regions are as steep as -0.9 , it is clear that the filament is non-thermal, particularly as parts of the filament have brightnesses at 90 cm in excess of $200 \text{ mJy beam}^{-1}$ or brightness temperatures of $> 7000 \text{ K}$. This cannot be formed by thermal emission at $\sim 10^4 \text{ K}$, as such gas would be optically thick and show a positive spectral index.

In addition to the filament there are at least three additional sources associated with Sgr C. At 18 cm the most prominent of these is G359.43-0.09 which has a shell-type structure, 2 arcmin in diameter, and a peak brightness of $230 \text{ mJy beam}^{-1}$. However, at 90 cm the total flux density of this region is $\sim 1 \text{ Jy}$ and its peak brightness is 57 mJy beam^{-1} . Hence the source has a positive spectral index consistent with optically thick thermal emission (i.e. $EM \sim 10^5 \text{ pc cm}^{-6}$). Much of the recombination line emission detected

from Sgr C with a 3.5-arcmin beam (Anantharamaiah & Yusef-Zadeh 1989) probably arises in this region. The southernmost source, G359.39-0.08, appears to have a relatively flat spectral index with a peak brightness of $\sim 100 \text{ mJy beam}^{-1}$ at 18 and 90 cm. We do not detect G359.47-0.17 ($< 30 \text{ mJy beam}^{-1}$) despite the fact that it has an 18-cm brightness of 70 mJy beam^{-1} which is consistent with it being thermal and optically thick at 90 cm. This source aligns closely with the linear filament of Sgr C, and could be physically associated. The lower-resolution CD image (Fig. 1) suggests that weak elongated emission may extend for at least 10 arcmin to negative latitudes.

The total flux density of Sgr C, measured above the 0.5-Jy contour of the low-resolution CD image, is 23 Jy, which is considerably greater than 9.8 Jy at 73 cm reported by Little (1974). Thus it appears that the source does not have a flat spectrum below 1 GHz as tabulated by Downes *et al.* (1978). The linear filament contributes ~ 30 per cent to this non-thermal component, whereas the remainder must originate from more extended structure. Presumably the spectrum is flat at high frequencies because most of the flux originates in the thermal component. The Sgr C filament has structure which is similar to at least two other linear features detected just to the north of this region. These are discussed in the next section.

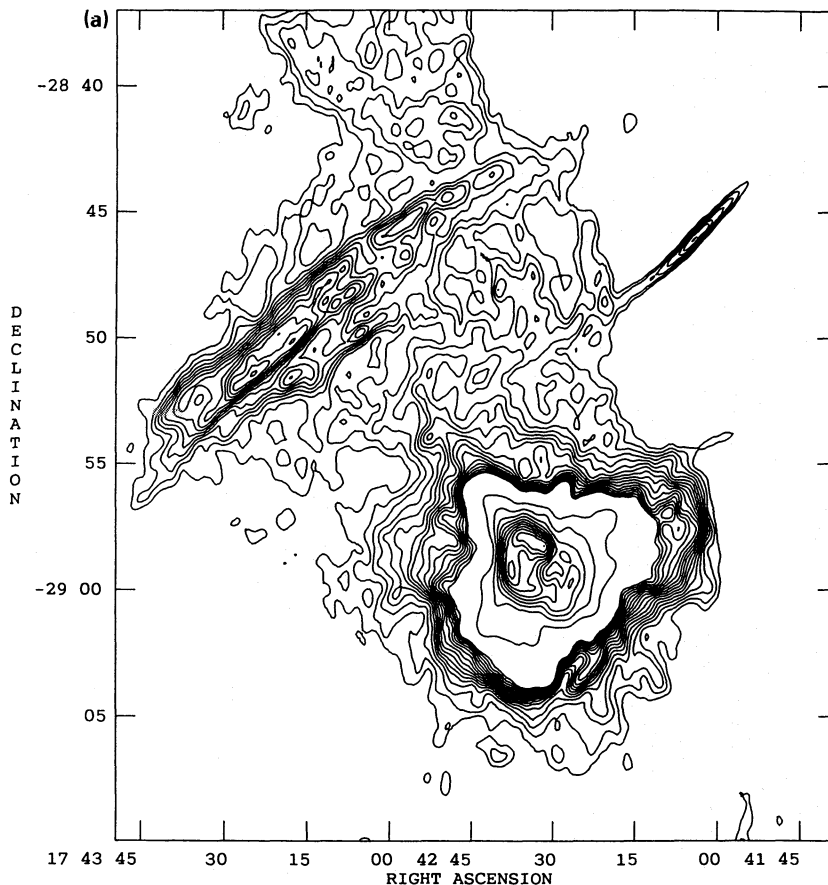


Figure 6. (a) A 90-cm sub-image of Fig. 2 showing the Arc and Sgr A. The angular resolution is $33 \times 17 \text{ arcsec}^2$. Contour levels are 80 to 400 in steps of 20, 400 to 5600 in steps of 400 mJy beam^{-1} . (b) A 20-cm image of the same region as (a), obtained from Yusef-Zadeh (1986) and convolved to the same resolution. Contour levels are $-50, 50$ to 750 in steps of 50, 1000 to 7000 in steps of 1000 mJy beam^{-1} . (c) The 90/20-cm spectral index distribution obtained from (a) and (b), superimposed as a grey-scale on the 90-cm contour map. The lightest regions correspond to $\alpha = 0$ and the darkest regions to $\alpha \geq 1$.

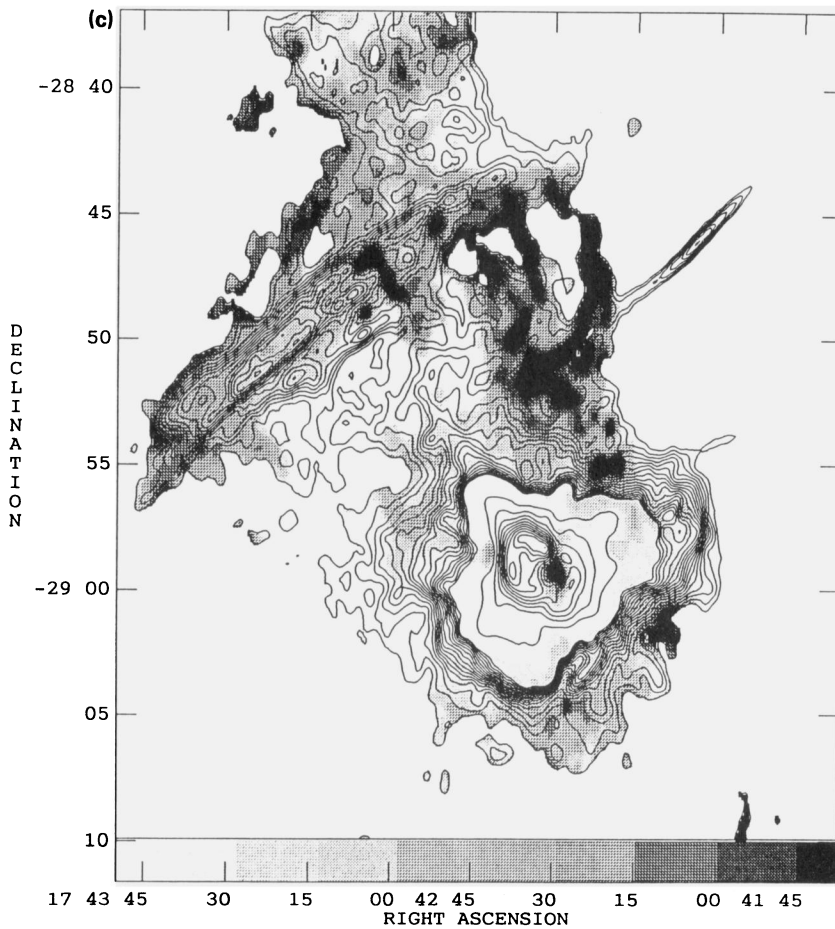
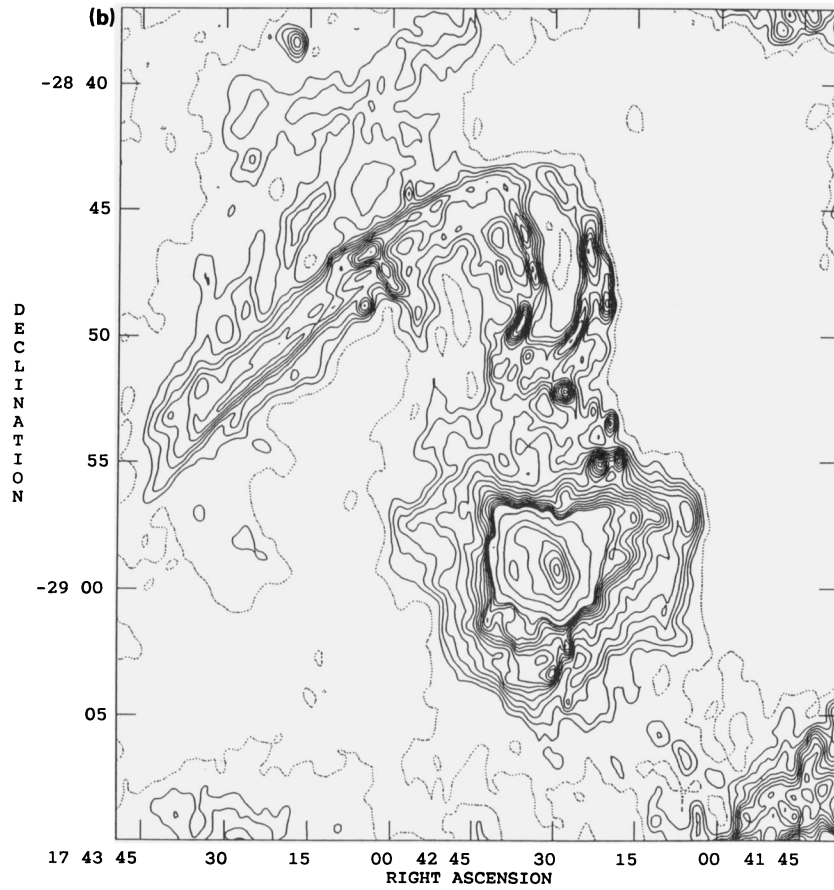


Figure 6 - continued

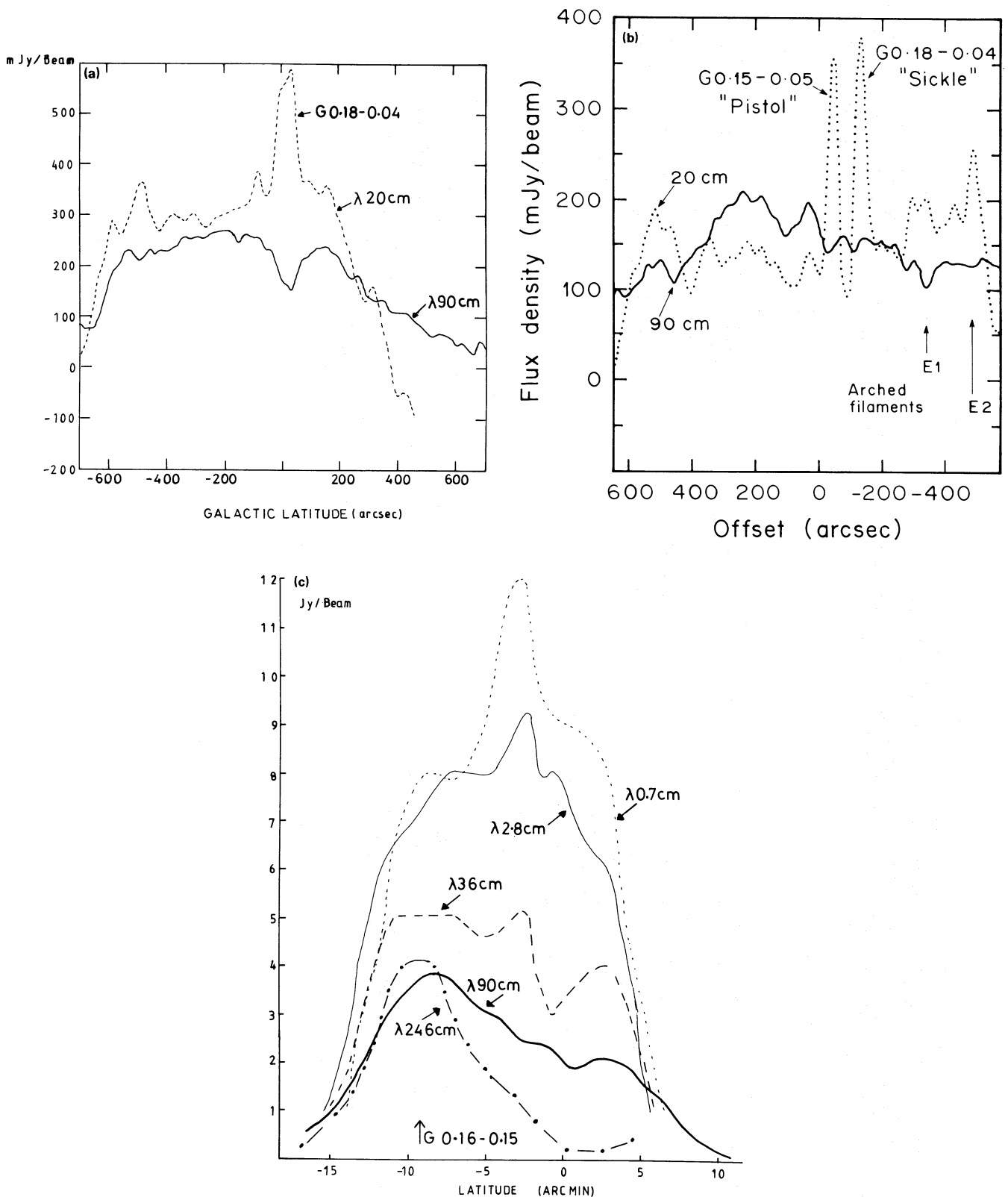


Figure 7. (a) Cross-cuts along the northern edge of the Arc, passing through G0.18–0.04, made from the images shown in Fig. 6(a) and (b). This figure shows the 90-cm absorption feature associated with G0.18–0.04. (b) Cross-cut along the southern edge of the Arc through the position of G0.15–0.05 ('pistol') and G0.18–0.04 ('sickle') at 90 and 20 cm, taken from Fig. 6(a) and (b), respectively. The cross-cut is centred at RA=17^h 43^m 9^s.6 and Dec.=–28° 49' 42" at a position angle of –50°. The positions at which the two eastern branches of the arched filaments intersect the Arc are also indicated. (c) Cross-cuts along the Arc at 0.7, 2.8, 36, 90 and 243 cm (43, 10.7 GHz, 843, 332 and 123 MHz). The three shortest wavelength cross-cuts were derived from the contour images by Reich *et al.* (1988) which, together with the 90-cm image, have been convolved to a common resolution of 1.5 arcmin. The 123-MHz cut was reconstructed from the contour map shown by Kassim *et al.* (1986), which has a resolution of 3.3 × 5.8 arcmin².

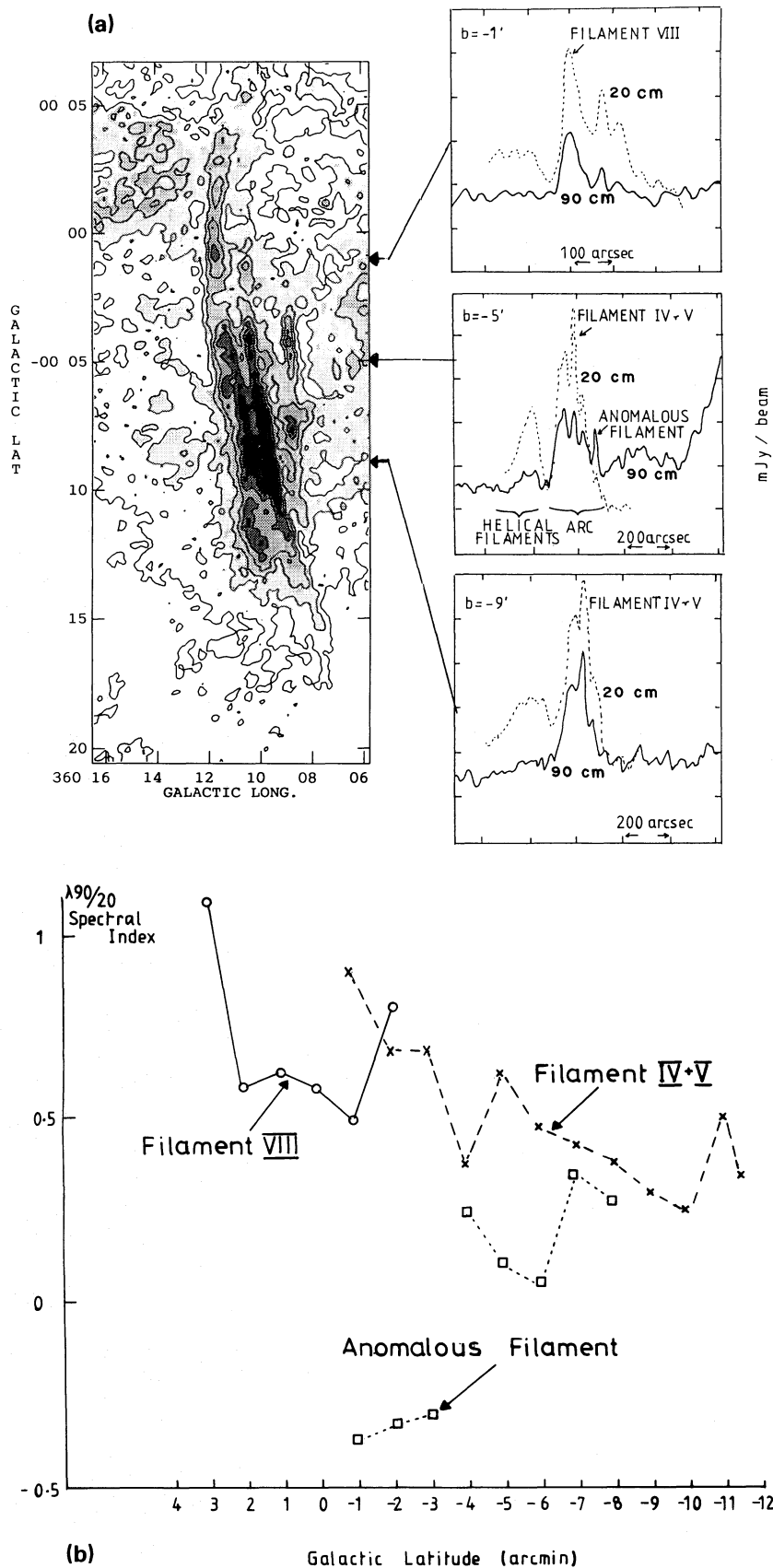


Figure 8. (a) A selection of cross-cuts across the Arc at 90 (solid lines) and 20 cm (dotted lines) at galactic latitudes $-0^{\circ}15$, $-0^{\circ}08$ and $-0^{\circ}02$ together with a subimage of Fig. 3. The cross-cuts were made after convolving the 90- and 20-cm images to a common resolution of 15 arcsec. The tic marks on the vertical axis of the cross-cuts are at intervals of 50 mJy beam^{-1} . (b) The spectral indices of three linear filaments of the Arc as a function of latitude along the filament. The spectral indices were derived from cross-cuts of which those shown in (a) are typical.

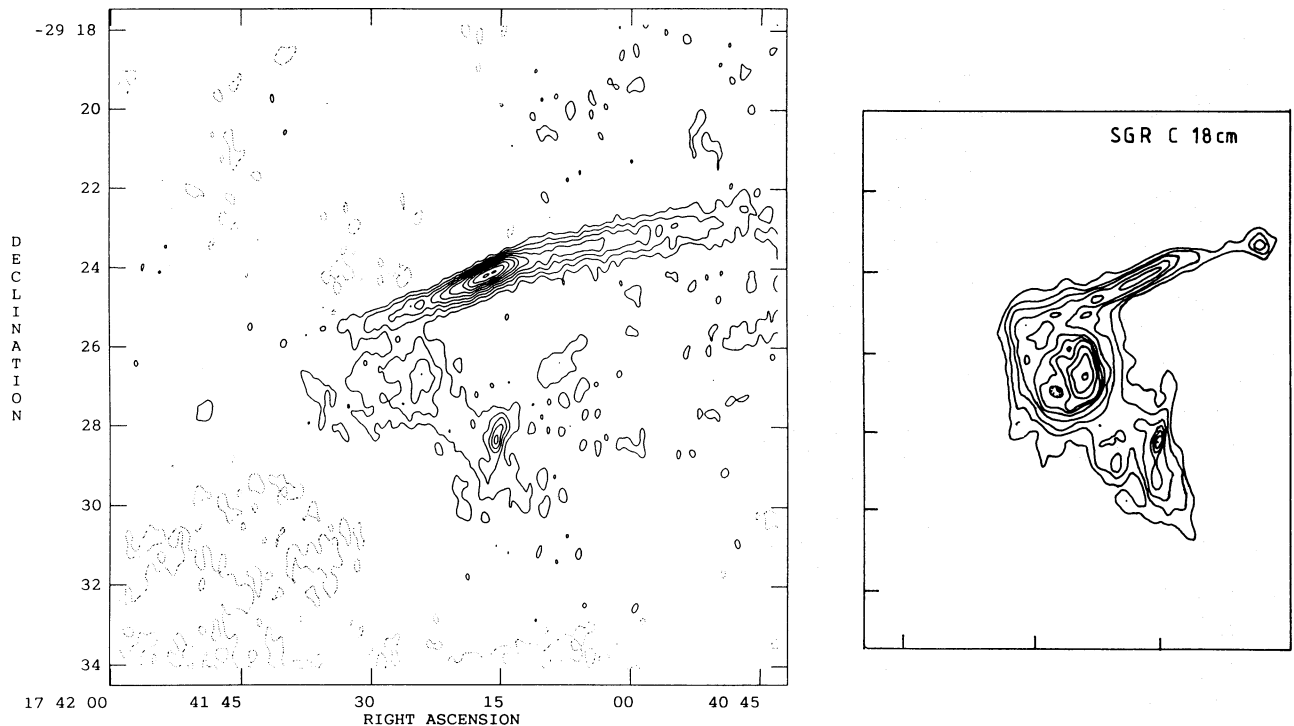


Figure 9. Left Panel: a contour image of Sgr C at 90 cm. This image was obtained from the AB UV data by shifting the field centre to the position of Sgr C. This procedure partially eliminates the effect of non-coplanar baselines. The contour levels are in units of $0.02 \text{ Jy beam}^{-1}$ and the restoring beam is $23 \times 13 \text{ arcsec}^2$. Right Panel: selected contours from the 18-cm image of Sgr C from Liszt (1985).

3.5 The ‘threads’ and related filaments

The threads are unusual structures first reported by Morris & Yusef-Zadeh (1985), and consist of fine filaments of radio emission extending over 30 pc in length, and yet having a width of less than 0.5 pc. Although relatively weak at 20 cm, they appear as prominently as the Arc at 90 cm (e.g. Figs 2 and 3). At least four elongated features are detected in the 90-cm image (see Fig. 2), all of which have counterparts at 20 cm (Morris & Yusef-Zadeh 1985; Bally & Yusef-Zadeh 1989a). Yusef-Zadeh (1989) has reviewed the properties of these filamentary structures. In Fig. 10, we show a portion of the BCD image which contains three of these features together with Sgr C. The similarity of Sgr C to the other features is evident. Although the term ‘threads’ has previously been applied (Morris & Yusef-Zadeh 1985) to only the two northernmost features (Figs 2 and 5), we shall use this term to include all four. To distinguish these features we use the standard galactic nomenclature, based on the position at the centre of each thread (see Fig. 5). In Table 2 we summarize the parameters. The spectral index estimates of three of the threads have been derived by comparing cross-cuts between the 90-cm image and the 20-cm image from Yusef-Zadeh (1986). The spectral index of G359.54+0.18 has been estimated from our measurement and the total flux density measurement by Bally & Yusef-Zadeh (1989a). From Table 2, it is immediately obvious that most of the linear filaments have much steeper spectral indices than those contained in the Arc. Only G359.96+0.09 (Fig. 5), which is close to the Sgr A complex, has a flat spectral index. The spectral index indicates that the threads are non-thermal.

An examination of the cross-cuts at 20 and 90 cm show that, for the northernmost filament (G0.08+0.15), the widths at 90 cm may be systematically larger. The observed widths (FWHM) at 90 cm, after correcting for the beam size, are in the range 20–25 arcsec, whereas at 20 cm the widths are unresolved. Although instrumental effects may contribute to this broadening, this behaviour could indicate either scatter broadening or greater transverse extent of low-energy electrons. Because of the larger width at 90 cm, the peaks of the cross-cuts indicate a 90/20-cm spectral index of -0.35 ± 0.07 , whereas the integrated flux densities give a spectral index of -0.6 ± 0.1 .

We have searched the $\sim 2^\circ \times 2^\circ$ field for evidence of more elongated features but have found no new detections. All these threads are found at positive latitudes, and hence their asymmetric distribution to the north of the plane does not seem to be a selection effect. As noted by Yusef-Zadeh (1989), it is interesting that these four features lie within the Ω -shaped lobe described by Sofue & Handa (1984), whose outer boundaries appear to be delineated by weak extensions to Sgr C and the Arc.

3.6 The north galactic lobe

LaRosa & Kassim (1985) and Kassim *et al.* (1986) have reported the detection, at wavelengths of 3.7, 2.7 and 2.4 m (80, 110 and 123 MHz), of an extended steep-spectrum source ~ 34 arcmin north-east of the Galactic Centre (see Fig. 5). They refer to this source as the northern galactic lobe (NGL) and Kassim *et al.* (1986) suggest that this steep-spectrum source represents Seyfert-like activity in the galactic

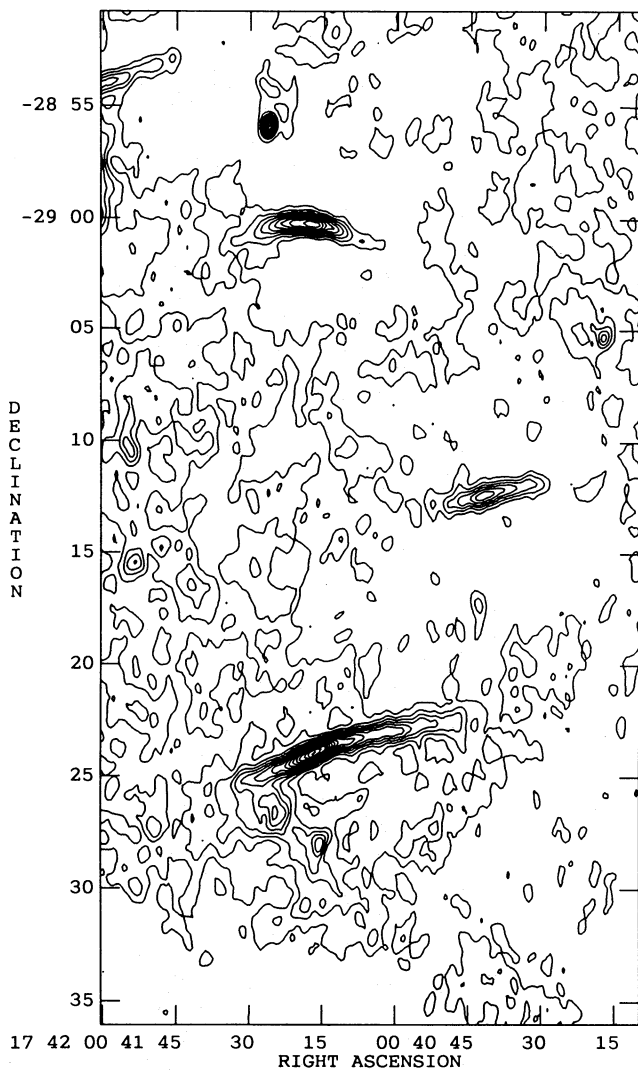


Figure 10. A subimage of Fig. 2 showing Sgr C and the filaments G359.54+0.18 and G359.79+0.17. The contour levels are 20 to 320 in steps of 20 mJy beam⁻¹.

Table 2. Parameters of the threads.

Thread G. No.	Length arcsec	Width arcsec	90-cm Peak	90/20 mean	B_{min} μG
			flux density mJy/beam	Spectral Index	
G0.08+0.15	390	21	200	-0.6±0.1	100
G359.96+0.09	265	26	90	-0.04±0.03	70
G359.79+0.17	185	35	190	-0.6±0.1	70
G359.54+0.18	215	40	130	-0.8±0.1 ^a	50
Sgr C	255	35	320	-0.55±0.4 ^b	100

^aEstimated from total flux density.

^b90/18-cm spectral index.

nucleus. Our observations reveal this region as an asymmetric shell-type structure, superimposed on an underlying ‘wedge’ of low-brightness emission with opening angle $\sim 30^\circ$. Although this feature is structurally similar to the north-western radio lobe in the Seyfert galaxy NGC 1068 (Ulves-

tad & Wilson 1984), in view of the high optical depth of the thermal gas at $\lambda \sim 3$ m in this area, it is clearly difficult to interpret the low-frequency images in terms of distinct components. It is perhaps premature to classify these components with those seen in Seyfert nuclei, which show a range of sizes and luminosities extending over several orders of magnitude (Unger *et al.* 1986). Furthermore, very steep spectra are not usually a property of such components. Indeed a number of them show relatively flat spectra at low frequencies which Pedlar *et al.* (1983, 1984) interpret as low-frequency turnovers indicative of free-free absorption.

It may indeed be more logical to view these emissions areas as ‘windows’ in the otherwise optically thick thermal gas. In fact, the NGL lies between the ionized gas of Sgr B1 and a region of ionized gas immediately to the south of this source (Anantharamaiah & Yusef-Zadeh 1989) as illustrated in Fig. 11. A non-uniform screen of thermal material in this region has in fact been suggested as a possible explanation for symmetrical polarization structures observed near the Arc (Seiradakis *et al.* 1985). In this case, Faraday depolarization by the thermal gas causes apparent structure in the polarized emission from an otherwise uniform synchrotron emitting region. Since no recombination measurements are available at the position of the NGL itself, the possibility that the NGL is a distinct foreground steep-spectrum object cannot be precluded.

3.7 The low-frequency jet

Yusef-Zadeh *et al.* (1986a) have reported the detection of a steep-spectrum ridge of radio emission at 190 cm (160 MHz), extending in the south-east direction from the galactic nucleus. They consider this as a low-energy jet emanating from the galactic nucleus. Further evidence for this feature has come from longer-wavelength observations by Kassim *et al.* (1986). We show in Fig. 11 selected contours of this ‘jet’ taken from Yusef-Zadeh *et al.* (1986a) and superimposed on our CD image. Clearly, we detect emission at all positions along the jet. From a morphological point of view, however, there is no obvious contrast between this region and its surroundings. For this reason, we do not find it compelling to consider this feature as a radio jet. The strength of this region at 90 cm is in the range 0.5–2.5 Jy beam⁻¹, and by comparison with the 190-cm emission (Yusef-Zadeh *et al.* 1986a), a spectral index of ~ -0.9 is obtained. The ‘low-frequency jet’ is observed only at wavelengths longer than 190 cm (160 MHz). In higher-resolution images of the Sgr A complex near 20 cm (Yusef-Zadeh & Morris 1987a) and 90 cm (see Fig. 3), there is a narrow ridge of emission extending about 2 arcmin from the shell of Sgr A East, at approximately the same position angle as the low-frequency jet. However, this emission appears to be a sub-structure in the 7-arcmin halo (see Paper I) and is unlikely to be connected with the low-frequency jet. This feature resembles one of the ‘north-west streamers’ discussed by Yusef-Zadeh & Morris (1987a).

As we have discussed above in relation to the NGL, the effect of thermal absorption at wavelengths longer than 1 m is considerable. In view of the fact that we do not see either the NGL or the low-frequency jet as distinct features at 90 cm, we stress that caution should be exercised in interpreting the structure of any feature observed only at long wavelengths.

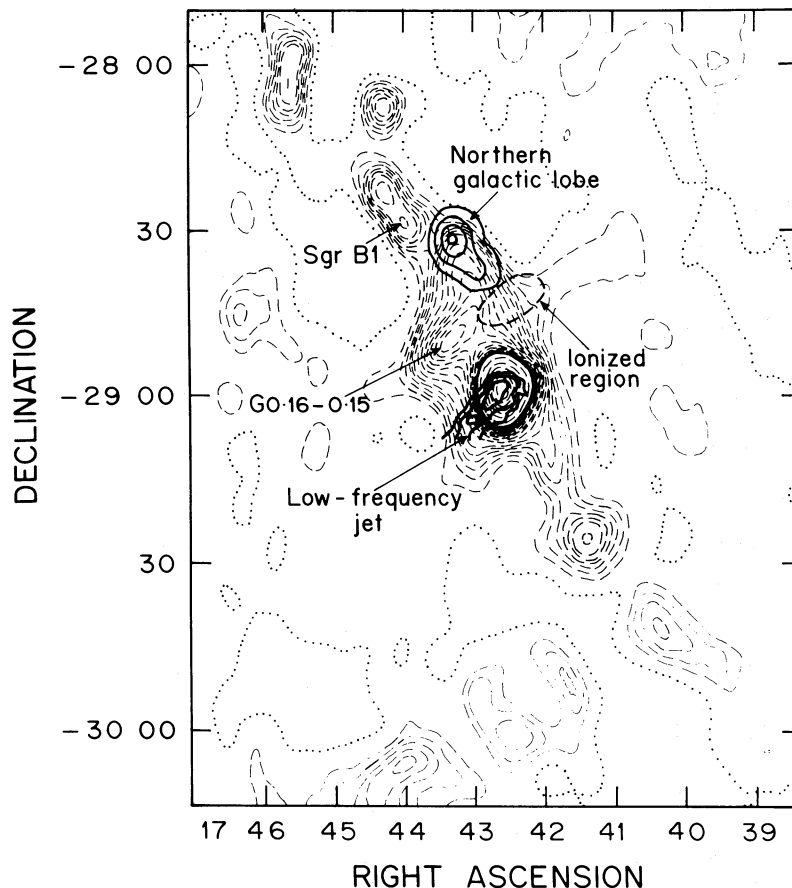


Figure 11. A 90-cm CD image convolved to the 3.3×5.8 -arcmin² resolution of Kassim *et al.* (1986). The contour levels are $-1, 1$ to 6 in steps of $1, 8$ to 30 in steps of 2 and 40 to 160 in steps of 20 Jy beam⁻¹. Selected contours of the 'north galactic lobe' from Kassim *et al.* (1986) and of the 'low-frequency jet' from Yusef-Zadeh *et al.* (1986a) are shown. The extent of the ionized region discussed in Sections 3.2 and 3.3 is also indicated.

If indeed the NGL and the low-frequency jet represent windows in the otherwise optically thick thermal gas, then their relatively steep spectra ($\alpha \leq -1.0$) suggest that the spectral index of the background radiation in the direction of the Galactic Centre is more negative than elsewhere in the galactic plane, where it has a value between -0.5 and -0.7 (Reich & Reich 1988; Dwarakanath 1989).

4 DISCUSSION

4.1 The poloidal magnetic field

Whereas the mechanism for producing the unique filamentary structures in the Galactic Centre region is not understood (see Yusef-Zadeh 1989), there is broad agreement that such structures must be the consequence of a substantial poloidal magnetic field which pervades the central ~ 100 pc of our Galaxy (Morris & Yusef-Zadeh 1989; Morris 1990, and references therein). The present observations reinforce this hypothesis, and the suggestion of a poloidal field is particularly compelling in Fig. 2, where the threads could be envisaged to be part of a dipole field. The Arc itself has the wrong curvature to be consistent with such a simple field. However, this may represent a local distortion caused, for example, by the interaction of a giant molecular

cloud. The minimum-energy approximation (Miley 1980) can be used to estimate the magnetic field in the threads. As the structure of the threads indicate that they are magnetically dominated, these values almost certainly represent lower limits. In Table 2 we give estimates of the fields in a number of components using this method. We have assumed that the depths of the filaments are equal to their mean widths, and that the energies in relativistic protons and electrons are equal. Typically we obtain values in excess of 50 – 100 μ G. Yusef-Zadeh & Morris (1987b,c) have argued that the field strength must exceed 1 mG in the Arc, and fields as high as 10 mG have been inferred for parts of Sgr A West (Werner *et al.* 1988; Aitken 1989). Recent measurements of the Zeeman effect in the 21-cm neutral hydrogen line have indicated that a 0.5 -mG field is present (Schwarz & Lasenby 1990). Searches for the Zeeman effect in 18-cm OH lines (Kilean *et al.* 1990) and in 3.6-cm recombination lines (Goss *et al.* 1990) have yielded upper limits to field strength near Sgr A West of 4 and 15 mG, respectively.

The origin of this poloidal field is unclear, although it could imply the existence of a dynamo near the Galactic Centre. Lesch *et al.* (1989) have proposed a mechanism to produce such a poloidal field in M82, whereby the outflow from central activity interacts with the dense molecular ring

to produce a ring current and a magnetic field. A similar mechanism, albeit on a smaller scale, could be operating in the Galactic Centre, although, as yet, the evidence is largely circumstantial.

4.2 On the spectral indices of the linear filaments and threads

As discussed in Section 3.3, many non-thermal features in the Galactic Centre show a flat, or even positive ($\alpha \sim +0.3$), spectral index. A mixture of thermal and non-thermal gas can produce a positive spectral index. Such a model was used in Paper I to explain the spectrum of the 7-arcmin halo near the Sgr A complex. There is evidence that some thermal emission is intimately associated with the Arc, as the linear filaments appear to be directly interacting with the thermal sources such as G0.18–0.04 and G0.15–0.05 (Yusef-Zadeh & Morris 1987b, 1988). In this model, the spectral index must change sign at some higher frequency as in the case of the 7-arcmin halo (Paper I). Since Reich *et al.* (1988) have observed a positive spectral index even above 10 GHz, it seems more likely that the positive spectral index is intrinsic to the non-thermal emission. If the non-thermal emission is due to the synchrotron mechanism, then a spectral index of $+0.3$ would imply that the power-law distribution of relativistic electrons follows an $E^{-0.4}$ power law (where E is the energy of the electrons), as compared to typical supernovae which show E^{-2} power laws. As the radio spectrum shows no steepening below 43 GHz (Reich *et al.* 1988), then, given fields of 1 mG, electrons with energies up to ~ 1.5 GeV are required, which have synchrotron lifetimes of $\sim 5 \times 10^3$ yr. Hence, to maintain the observed spectrum, the electrons would need to be re-accelerated on such time-scales. As pointed out by Reich *et al.* (1988), the positive spectral indices can also be explained if the electrons have a mono-energetic spectrum or have a low-energy cutoff.

As was discussed in Section 3.3, however, at least one of the linear filaments in the Arc shows a relatively steep 90/20-cm spectral index ($\alpha \sim -0.4$). It also shows $a \sim 10^\circ$ misalignment from most of the other filaments in this part of the Arc. The anomalous properties of this filament may, in some part, be due to its position at the innermost edge of the Arc, although the steep spectral index can be explained if the filament has been disconnected from the source of relativistic electrons and is evolving as a typical synchrotron source. Since the 0.3-GeV electrons (which are responsible for the 20-cm emission) have synchrotron lifetimes of $\sim 3 \times 10^4$ yr, we could postulate that no large input of relativistic electrons has occurred on this time-scale.

The steep spectrum of three of the ‘threads’ (Section 3.5) may also indicate that no source of relativistic particles is currently present, and the threads represent relics of activity which took place $> 3 \times 10^4$ yr ago. We could speculate that G359.96+0.09 (the flat-spectrum thread) represents the young phase of these objects. As these threads are typically 30 pc from the plane, we could also speculate that these filaments propagate along magnetic field lines away from the plane. Given the above lifetimes, this would imply a mildly relativistic propagation velocity of $\sim 10^5$ km s $^{-1}$. It may be significant that the threads, the linear filaments of the Arc, and the filament in Sgr C have orientations roughly parallel to the axis of galactic rotation. This will allow them to retain their linear structure for long times ($> 10^7$ yr) in spite of

strong differential galactic rotation in this region (see also Yusef-Zadeh *et al.* 1984).

4.3 Speculations on particle acceleration

Flat non-thermal spectra are usually found in objects such as the Crab nebula, where there is continuous generation of relativistic particles from a central energy source. Following this analogy, it appears that the flat and positive spectrum non-thermal features are directly associated with a source of relativistic particles. It is tempting to associate the source of these particles with the compact source Sgr A*, which itself has a positive spectral index ($\alpha \sim +0.3$, Lo 1987). Then the linear filaments could represent ‘traps’ for such particles, although this would require that the charged particles travel ~ 50 pc against the poloidal field, and it is surprising that no trail is left behind. Furthermore, there is evidence (see Paper I) that the diffuse non-thermal component in the Sgr A complex has a steep spectrum, indicating that significant synchrotron ageing has occurred even within 10 pc of the nucleus. In view of these difficulties we prefer models in which the electrons are accelerated locally (i.e. in the Arc and in G359.96+0.09) and propagate along the poloidal fields.

Benford (1988) has proposed that molecular clouds moving through the poloidal field will induce strong electric fields, which can then drive currents and accelerate particles in the interstellar medium. A cloud moving at a velocity of 50 km s $^{-1}$ in a magnetic field of 1 mG, induces a $\mathbf{v} \times \mathbf{B}$ electric field of 5×10^{-3} V m $^{-1}$. If these fields can be maintained over distances of $\sim 10^{13}$ m, then electrons with energies of a few GeV, which are necessary for the radio emission, could be produced. The association of molecular cloud complexes with the filaments in the Arc, Sgr C and G358.54+0.18 provides some circumstantial evidence in favour of this model (Bally & Yusef-Zadeh 1989b), although at least one of the threads (G359.79+0.17) does not have an associated molecular cloud (see fig. 1 in Bally & Yusef-Zadeh 1989b). The detailed implications of this type of mechanism are yet to be fully investigated. Other mechanisms have been summarized by Yusef-Zadeh (1989).

There may be an association of ‘flat’ spectrum linear features with violent thermal activity. This occurs in the Arc, which is associated with thermal emission in G0.18–0.04 and G0.15–0.05, which Yusef-Zadeh, Morris & van Gorkom (1987, 1989) have shown to emit recombination line emission with widths as large as 90 km s $^{-1}$. It is interesting to note that one of the filaments which does not have a flat spectrum is not physically associated with G0.18–0.04. The structure of the helical thermal structures also indicates a close connection between thermal and non-thermal emission in the Arc. The thread G359.96+0.09 may be associated with thermal emission in the 7-arcmin halo of Sgr A. Hence we might surmise that, in these cases, the thermal emission is in some way associated with, or is a byproduct of, the acceleration mechanism responsible for the relativistic electrons. A direct connection between the two types of emission has in fact been suggested by Yusef-Zadeh & Morris (1987b), where the thermal gas is a result of ionization by lower-energy relativistic electrons. If the initial energy spectrum of the electrons is the usual power law (E^{-2}), then, due to the loss of the lower-energy electrons to ionization, the resultant electron energy spectrum could be flat. Such a

mechanism would simultaneously explain the slightly positive spectral index of some of the filaments and their association with thermal gas.

5 CONCLUSIONS

We have observed the Galactic Centre region at 90 cm in the A, B, C and D configurations of the VLA. Using different subsets of these data we have made three images with different resolution and field sizes. The first is a low-resolution image (100×64 arcsec²) made using the C and D configuration data and covers a field of $2^\circ \times 2^\circ$ around the Galactic Centre. An intermediate resolution image (33×17 arcsec²), made using the B, C and D configuration data, covers a field of $1^\circ \times 1^\circ$. Finally, a high-resolution (14×9 arcsec²) image made using the A and B configuration data covers the central 30-arcmin region which includes the Sgr A complex and the Arc.

By comparing these images with those at other frequencies (e.g. Yusef-Zadeh *et al.* 1984; Morris & Yusef-Zadeh 1985; LaRosa & Kassim 1985; Yusef-Zadeh *et al.* 1986a; Yusef-Zadeh & Morris 1987a,b,c; Bally & Yusef-Zadeh 1989a), we have studied the nature of several radio features associated with the Galactic Centre. The main results can be summarized as follows.

(i) All the unique structures associated with the Galactic Centre, which are detected at higher frequencies, such as the Sgr A complex, the Arc and its linear filaments, the thermal arched filaments, the 'threads' and other linear structures and Sgr C are present at 90 cm.

(ii) In the Sgr A complex, Sgr A West is in absorption against Sgr A East and confirms the conclusions of Paper I. The chain of H II regions to the east of Sgr A East show marginal absorption suggesting that they may be in front of the 7-arcmin halo (Paper I) or embedded in it.

(iii) A marked difference at 90 cm, compared to 20 cm, is a depression in the intensity of the arched filaments and the positive latitude part of the Arc. This difference is attributed to the fact that thermal gas present in these regions becomes optically thick at 90 cm. While the arched filaments themselves are thermal (Yusef-Zadeh *et al.* 1987) and become optically thick at 90 cm, we attribute the decrease in the intensity of the Arc at positive latitudes to the presence of an extended region of ionized gas with $\tau \sim 1$ at 90 cm.

(iv) With the exception of the southernmost filament in the Arc, all the other linear filaments in this region show a flat or positive 90/20-cm spectral index. Comparison with shorter-wavelength measurements indicate that this spectral index is intrinsic and not caused by free-free absorption. The southern filament has a spectral index of -0.4 , and is out of alignment with the other parallel filaments of the Arc.

(v) The northernmost filament in the Arc does not show a decrease in intensity, indicating that it may be on the near side of the extended ionized region.

(vi) The 'sickle' feature (G0.18 - 0.04), which crosses the Arc at right angles is seen in absorption at 90 cm. This clearly shows that it is situated on the near side of the Arc. The pistol-shaped feature (G0.15 - 0.05) shows marginal absorption, suggesting that it may also be in front of the Arc.

(vii) The position at which the eastern and western branches of the arched filaments meet the Arc, show only marginal absorption and it is not possible to decide whether

these are in front of the Arc. The geometry of this region is further confused by the presence of an extended ionized region which also becomes optically thick at 90 cm.

(viii) The brightness temperature of the linear filaments in the Arc is > 5000 K, which, given that their spectrum is not consistent with optically thick thermal emission, confirms their non-thermal nature.

(ix) When seen on a single large-field image (Fig. 2), the 'threads' (Morris & Yusef-Zadeh 1985), Sgr C (Liszt 1985) and other linear features in this region (e.g. Bally & Yusef-Zadeh 1989a) appear to have similar structures. These can be thought of as tracing a dipolar magnetic field in this region. Using the minimum-energy approximation (Miley 1980), we obtain lower limits of 50–100 μ G for the magnetic field in these features.

(x) The threads and related features appear to be situated only at positive latitudes. We find no new threads at 90 cm. Compared to 20 cm, the northernmost thread (G0.08 + 0.15) appears to have a systematically larger width at 90 cm all along its length.

(xi) Most of the linear filaments in the Arc and the 'thread' G359.96 + 0.09 have a flat or positive spectral index, whereas the other 'threads' and the filament of Sgr C show negative spectral indices. The positive or flat spectral index of the linear filaments require that relativistic electrons must be produced, possibly *in situ*, on time-scales of $\sim 10^4$ yr. There appears to be an association of flat or positive spectral index linear filaments with violent thermal activity.

(xii) The radio features detected at very long wavelengths, namely the northern galactic lobe (LaRosa & Kassim 1985) and the 'low-frequency jet' (Yusef-Zadeh *et al.* 1986a) do not show up as distinct features at 90 cm, although we detect emission at the position of these features. We suggest that the appearance of these regions as distinct features at long wavelengths is due to the patchiness of optically thick thermal gas which is widespread in this area.

ACKNOWLEDGMENTS

We acknowledge the major contribution of Jacqueline van Gorkom to this project. We are grateful to Farhad Yusef-Zadeh both for providing a 20-cm image and for many discussions on several aspects of the Galactic Centre radio emission. We also had useful discussions with Patrick Leahy, Wolfgang Reich, Ko Hummel and Chris Salter. KRA thanks NRAL, Jodrell Bank for a SERC grant and hospitality during part of this work.

REFERENCES

- Aitken, D. K., 1989. In: *The Center of the Galaxy, IAU Symp. 136*, p. 457, ed. Morris, M., Kluwer, Dordrecht.
- Altenhoff, W. J., Downes, D., Pauls, T. & Schraml, J., 1978. *Astr. Astrophys. Suppl.*, **35**, 23.
- Anantharamaiah, K. R. & Yusef-Zadeh, F., 1989. In: *The Center of the Galaxy, IAU Symp. 136*, p. 159, ed. Morris, M., Kluwer, Dordrecht.
- Bally, J. & Yusef-Zadeh, F., 1989a. *Astrophys. J.*, **336**, 173.
- Bally, J. & Yusef-Zadeh, F., 1989b. In: *The Center of the Galaxy, IAU Symp. 136*, p. 189, ed. Morris, M., Kluwer, Dordrecht.
- Benford, G., 1988. *Astrophys. J.*, **333**, 735.

- Bridle, A. H., 1989. In: *Synthesis Imaging in Radio Astronomy*, p. 433, eds Perley, R. A., Schwab, F. R. & Bridle, A. H., Astronomical Society of the Pacific, San Francisco.
- Brown, R. L., Johnston, K. J. & Lo, K. Y., 1981. *Astrophys. J.*, **250**, 155.
- Cornwell, T. J. & Evans, K. F., 1985. *Astr. Astrophys.*, **89**, 377.
- Cotton, W. D., 1989. In: *Synthesis Imaging in Radio Astronomy*, p. 233, eds Perley, R. A., Schwab, F. R. & Bridle, A. H., Astronomical Society of the Pacific, San Francisco.
- Downes, D., Goss, W. M., Schwarz, U. J. & Wouterloot, J. G. A., 1978. *Astr. Astrophys. Suppl.*, **35**, 1.
- Dwarakanath, K. S., 1989. *PhD thesis*, Indian Institute of Science, Bangalore.
- Ekers, R. D., van Gorkom, J. H., Schwarz, U. J. & Goss, W. M., 1983. *Astr. Astrophys.*, **122**, 143.
- Gopal-Krishna, Swarup G., Sarma, N. V. G. & Joshi, M. N., 1972. *Nature*, **239**, 91.
- Goss, W. M., van Gorkom, J. H., Roberts, D. A. & Leahy, J. P., 1990. In: *Radio Recombination Lines – 25 Years of Investigations*, IAU Coll. 125, p. 249, eds Gordon, M. A. & Soroichenko, R. L., Kluwer, Dordrecht.
- Inoue, M., Takahashi, T., Tabara, H., Kato, T. & Tsuboi, M., 1984. *Pubs astr. Soc. Japan*, **36**, 633.
- Inoue, M., Fomalont, E., Tsuboi, M., Yusef-Zadeh, F., Morris, M., Tabara, H. & Kato, T., 1989. In: *The Center of the Galaxy*, IAU Symp. 136, p. 269, ed. Morris, M., Kluwer, Dordrecht.
- Kassim, N. E., LaRosa, T. N. & Erickson, W. C., 1986. *Nature*, **322**, 522.
- Kellermann, K. I. & Wall, J. V., 1987. In: *Observational Cosmology*, p. 545, eds Hewitt, A., Burbidge, G. & Li Zhi Fang, D., Reidel, Dordrecht.
- Kesteven, M. J. & Pedlar, A., 1977. *Mon. Not. R. astr. Soc.*, **180**, 731.
- Kileen, N. E. B., Lo, K. Y., Sault, R. J. & Crutcher, R. M., 1990. In: *Galactic and Intergalactic Magnetic Fields*, IAU Symp. 140, p. 382, eds Beck, R., Kronberg, P. P. & Wielebinski, R., Kluwer, Dordrecht.
- LaRosa, T. N. & Kassim, N. E., 1985. *Astrophys. J.*, **299**, L13.
- Lesch, H., Crusius-Watzel, A., Schlickeiser, R. & Wielebinski, R., 1989. *Astr. Astrophys.*, **217**, 99.
- Liszt, H. S., 1985. *Astrophys. J.*, **293**, L65.
- Little, A. G., 1974. In: *Galactic Radio Astronomy*, p. 491, eds Kerr, F. J. & Simonson, S. C., Reidel, Dordrecht.
- Lo, K. Y., 1987. In: *The Galactic Center, Townes Symposium*, p. 30, ed. Backer, D. C., American Institute of Physics, New York.
- Miley, G., 1980. *Ann. Rev. Astr. Astrophys.*, **18**, 165.
- Mills, B. Y. & Drinkwater, M. J., 1984. *J. Astrophys. astr.*, **5**, 43.
- Morris, M., 1990. In: *Galactic and Intergalactic Magnetic Fields*, IAU Symp. 140, p. 361, eds Beck, R., Kronberg, P. P. & Wielebinski, R., Kluwer, Dordrecht.
- Morris, M. & Yusef-Zadeh, F., 1985. *Astr. J.*, **90**, 2511.
- Morris, M. & Yusef-Zadeh, F., 1989. *Astrophys. J.*, **343**, 703.
- Pauls, T. & Mezger, P. G., 1980. *Astr. Astrophys.*, **85**, 26.
- Pauls, T., Downes, D., Mezger, P. G. & Churchwell, E., 1976. *Astr. Astrophys.*, **46**, 407.
- Pedlar, A., Booler, R. V. & Unger, S. W., 1984. *Mon. Not. R. astr. Soc.*, **207**, 193.
- Pedlar, A., Booler, R. V., Spencer, R. E. & Stewart, O. J., 1983. *Mon. Not. R. astr. Soc.*, **202**, 647.
- Pedlar, A., Anantharamaiah, K. R., Ekers, R. D., Goss, W. M., van Gorkom, J. H., Schwarz, U. J. & Zhao, J., 1989. *Astrophys. J.*, **342**, 769 (Paper I).
- Perley, R., 1989. In: *Synthesis Imaging in Radio Astronomy*, p. 259, eds Perley, R. A., Schwab, F. R. & Bridle, A. H., Astronomical Society of the Pacific, San Francisco.
- Reich, P. & Reich, W., 1988. *Astr. Astrophys. Suppl.*, **74**, 7.
- Reich, W., 1990. In: *Galactic and Intergalactic Magnetic Fields*, IAU Symp. 140, p. 369, eds Beck, R., Kronberg, P. P. & Wielebinski, R., Kluwer, Dordrecht.
- Reich, W. & Fürst, E., 1984. *Astr. Astrophys. Suppl.*, **57**, 165.
- Reich, W., Sofue, Y., Wielebinski, R. & Seiradakis, J. H., 1988. *Astr. Astrophys.*, **191**, 303.
- Schwarz, U. J. & Lasenby, J., 1990. In: *Galactic and Intergalactic Magnetic Fields*, IAU Symp. 140, p. 383, eds Beck, R., Kronberg, P. P. & Wielebinski, R., Kluwer, Dordrecht.
- Seiradakis, J. H., Lasenby, A. N., Yusef-Zadeh, F., Wielebinski, R. & Klein, U., 1985. *Nature*, **317**, 679.
- Sofue, Y. & Handa, T., 1984. *Nature*, **310**, 568.
- Steer, D. G., Dewdney, P. E. & Ito, M. R., 1984. *Astr. Astrophys.*, **137**, 159.
- Thompson, A. R., 1989. In: *Synthesis Imaging in Radio Astronomy*, p. 11, eds Perley, R. A., Schwab, F. R. & Bridle, A. H., Astronomical Society of the Pacific, San Francisco.
- Thompson, A. R., Clark, B. G., Wade, C. M. & Napier, P. J., 1980. *Astrophys. J. Suppl.*, **44**, 151.
- Ulvestad, J. S. & Wilson, A. S., 1984. *Astrophys. J.*, **285**, 439.
- Unger, S. W., Pedlar, A., Booler, R. V. & Harrison, B. A., 1986. *Mon. Not. R. astr. Soc.*, **219**, 387.
- Werner, M. W., Davidson, J. A., Morris, M., Novak, G., Platt, S. R. & Hildebrand, R. H., 1988. *Astrophys. J.*, **333**, 729.
- Yusef-Zadeh, F., 1986. *PhD thesis*, University of Columbia.
- Yusef-Zadeh, F., 1989. In: *The Center of the Galaxy*, IAU Symp. 136, p. 243, ed. Morris, M., Kluwer, Dordrecht.
- Yusef-Zadeh, F. & Morris, M., 1987a. *Astrophys. J.*, **320**, 545.
- Yusef-Zadeh, F. & Morris, M., 1987b. *Astr. J.*, **94**, 1178.
- Yusef-Zadeh, F. & Morris, M., 1987c. *Astrophys. J.*, **322**, 721.
- Yusef-Zadeh, F. & Morris, M., 1988. *Astrophys. J.*, **329**, 729.
- Yusef-Zadeh, F., Morris, M. & Chance, D., 1984. *Nature*, **310**, 557.
- Yusef-Zadeh, F., Morris, M. & van Gorkom, J. H., 1987. In: *The Galactic Center, Townes Symposium*, p. 190, ed. Backer, D. C., American Institute of Physics, New York.
- Yusef-Zadeh, F., Morris, M. & van Gorkom, J. H., 1989. In: *The Center of the Galaxy*, IAU Symp. 136, p. 275, ed. Morris, M., Kluwer, Dordrecht.
- Yusef-Zadeh, F., Morris, M., Slee, O. B. & Nelson, G. J., 1986a. *Astrophys. J.*, **300**, L47.
- Yusef-Zadeh, F., Morris, M., Slee, O. B. & Nelson, G. J., 1986b. *Astrophys. J.*, **310**, 689.

APPENDIX A: DATA REDUCTION

A1 Imaging problems

Radio images of large fields at low frequencies will have distortions due to finite bandwidth, integration times and non-coplanar baselines. These distortions increase with distance from the field centre. Although the distortions due to finite bandwidth and time averaging can be overcome by using short integration times and multiple narrow bands, the effect of non-coplanar baselines present a more intractable problem. Thompson (1989) gives the approximate criterion for the non-coplanar distortions to be small as $\theta_F < \frac{1}{3} \theta_s^{1/2}$, where θ_s is the half-power width of the synthesized beam (in radians) and θ_F is the distance from the field centre. When applied to the present observations, the criterion suggests that we expect problems beyond $0^{\circ}4$ from the field centre for the lower resolution images (C array) decreasing to $0^{\circ}15$ for the highest resolution images (A array). This problem can be overcome, to some extent, by re-imaging the sources outside the central region by using sub-fields with the phase centres shifted to the location of the source. Although this technique works tolerably well for compact sources, there are difficulties in obtaining good images of extended sources and

improved imaging algorithms (i.e. 3D FFT, etc.) are required to overcome this problem fully (Perley 1989). In order to check the effect of non-coplanar baselines, we made sub-images of some sources outside the central region using shifted phasecentres. To reduce the effect of sidelobes from Sgr A, the central region containing the Sgr A complex and the Arc was cleaned and the ‘clean components’ were subtracted from the UV data before making the sub-images. A comparison between these sub-images and the original (i.e. large field) image, showed that only small distortions were introduced at \sim twice as far from the field centre as suggested by the criterion of Thompson (1989). Hence, single large fields derived from compact C and D array data gave reasonable images up to $\sim 1^\circ$ from the field centre. At the highest resolution using the A and B array data, a single field could be used to study both Sgr A and the Arc, which are separated by ~ 15 arcmin.

A2 The lower-resolution images

For imaging over a field of radius $\sim 1^\circ$, using spacings up to 9000λ (i.e. B, C and D configurations), the requirement of bandwidth and integration times are not stringent, and hence it is possible to form adequate images without resort to spectral line databases. An examination of the 10-s-integration data in the B configuration showed that the ionospheric phase was stable enough to allow averaging up to 30 s without loss of coherence. Hence, we averaged in both time and frequency to obtain a pseudo-continuum database with an effective bandwidth of 1.36 MHz and an integration time of 30 s. Using these parameters, the expected bandwidth and time-averaging smearing at 1° away from the field centre, is less than 5 per cent for B array observations (Bridle 1989). A description of the C and D configuration observations, calibration and their initial reduction was presented in Paper I. The image presented in Paper I was improved considerably by further self-calibration iterations, and independent use of the maximum-entropy (MEM) deconvolution technique (Cornwell & Evans 1985) in addition to the Steer-Dewdney-Ito (SDI) CLEAN algorithm (Steer, Dewdney & Ito 1984). The final ‘CD’ image, corrected for primary beam attenuation, is shown in Fig. 1. The angular resolution of this image is 100×64 arcsec², and the cell size is 20 arcsec. The effect of non-coplanar baseline was investigated using multiple sub-fields centred on the individual sources located near the edge of the field. G1.1–0.1 and the SNR shell G 359.1–0.5 showed some evidence of distortion, whereas Sgr C and Sgr B2 appeared relatively unaffected. The point source G358.9+0.1 ($\sim 1^\circ$ from field centre) showed little distortion and hence non-coplanar baseline effects do not seriously degrade the image within the central degree. A further shortcoming of this image is the lack of spacings $< 100 \lambda$, which results in insensitivity to extended structure on scales > 30 arcmin. The MEM and SDI deconvolution methods agreed well on scales less than 30 arcmin, although the MEM technique estimated the extended flux density from the missing low-order spacings. The negative regions in the SDI image shown in Fig. 1 are a direct result of this lack of low-order spacings. The rms noise in this image is ~ 60 mJy beam⁻¹ resulting in a dynamic range of $\sim 700:1$.

The B-configuration data were averaged in frequency to give a bandwidth of 1.36 MHz, and self-calibrated in phase

before being combined with the self-calibrated C- and D-configuration data. The combined data were used to obtain a $2^\circ \times 2^\circ$ image using the SDI CLEAN algorithm. This image with an angular resolution of 33×17 arcsec², is shown in Fig. 2. A grey-scale representation of the inner part of this image is shown in Plate 1. In order to check any distortions due to non-coplanar baselines on sources far away from the field centre, we made images of Sgr C and G358.9+0.1 ($\sim 0.5^\circ$ and $\sim 1.0^\circ$ from the field centre, respectively) by shifting the field centre to the position of these sources. We noted that the non-coplanar baseline effects produced only small distortions in Sgr C (see Fig. 3) whereas the distortion in the source G358.9+0.1 was considerable. Hence it appears that non-coplanar baseline problems do not cause serious distortions in structures out to 0.6° from the field centre. The rms noise in this image is ~ 7 mJy beam⁻¹, which gives a dynamic range of 650:1.

The large field ($2^\circ \times 2^\circ$) covered by the BCD image is expected to contain several background extragalactic sources. From the radio source counts at 408 MHz (Kellermann & Wall 1987), we expect, in a 4-deg² area, 0.9 sources with flux density exceeding 1 Jy, 2.3 sources exceeding 0.5 Jy, 12 sources exceeding 100 mJy and 15.5 sources exceeding 50 mJy. The strongest compact source in the BCD image is located at $\alpha = 17^{\text{h}} 38^{\text{m}} 31.7^{\text{s}}$, $\delta = -29^\circ 47' 54''$ and has a peak brightness of 970 mJy beam⁻¹. The point source which is indicated in Fig. 5 has an integrated flux density of 580 mJy. Two other compact sources are seen at $\alpha = 17^{\text{h}} 45^{\text{m}} 56^{\text{s}}$, $\delta = -28^\circ 22' 9''$ and $\alpha = 17^{\text{h}} 43^{\text{m}} 57.8^{\text{s}}$, $\delta = -28^\circ 33' 36''$ and have integrated flux densities of 790 and 310 mJy, respectively. All these are presumably extragalactic background sources. In addition to these relatively strong sources, at least 30 other compact features with peak brightness exceeding 50 mJy beam⁻¹ can be identified in the BCD image. Some of these may be galactic in origin. It therefore appears that the background extragalactic sources around the Galactic Centre has a distribution similar to other regions of the sky.

A3 The high-resolution image

The A and B array observations were made in 1988 December and 1989 March in dual-frequency spectral line mode and included all 27 VLA antennas. The centre frequencies were chosen to be 333.1 and 323.1 MHz. At an early stage it became clear that the 323.1-MHz observations were of lower quality than those at 333.1 MHz, and hence only the latter were included in the final images. Eight spectral line channels, each of width 195 kHz with an integration time of 10 s were used in both the configurations. The data were taken in this mode to allow imaging over the entire primary beam, without introducing significant time or bandwidth smearing. The amplitude was calibrated using 3C 286. The instrumental and ionospheric phase was calibrated using observations of the sources 1830–210 and 1827–360 at intervals of 15 min.

Attempts to self-calibrate the spectral line databases were not successful due to the poor signal-to-noise ratio on individual channels. Hence the A and B data sets were self-calibrated using the broad-band data which are recorded as ‘channel-zero’ data in the spectral line mode of the VLA.

Although the channel-zero data had a bandwidth of 4.7 MHz, they were useful in obtaining a good 'first model' of the central region since it dominates the continuum emission. (This method would not, of course, be possible in the presence of strong sources far away from the field centre. In addition the data were not affected by interference). The phase corrections obtained from the final self-calibration of the channel-zero data were applied to all the spectral line channels, before combining the two databases. All the spectral line channels of the combined data were simultaneously gridded and Fourier transformed to obtain a 'dirty' beam and a dirty image. Fortunately, most of the flux density in the Galactic Centre region is concentrated in the central 0.5, and, at the dynamic ranges achieved, we did not appear to be

significantly affected by strong confusing sources outside this region. This considerably simplified the data reduction. Both MEM and SDI CLEAN algorithms were used to deconvolve the image independently. Although both the deconvolved images were consistent in the outer regions, the SDI CLEAN image showed some evidence of clean instabilities in the central region. In order to reduce non-coplanar distortions over the Arc and Sgr A, the phase centre was placed between these two components, and a 20-k λ taper was applied to the UV data. In Fig. 3 (contours) and Plate 2 (grey-scale), we show the resulting image, deconvolved using MEM, which has been restored with a 14×9 -arcsec² beam. The rms noise in this image is 3 mJy beam⁻¹, which is close to the theoretically expected noise; the dynamic range is $\sim 200:1$.